nature methods

ARTICLES

https://doi.org/10.1038/s41592-020-0826-8

Check for updates

Pooled CRISPR screens with imaging on microraft arrays reveals stress granule-regulatory factors

Emily C. Wheeler[1,2,7], Anthony Q. Vu[1,2,7], Jaclyn M. Einstein[1,2], Matthew DiSalvo[3], Noorsher Ahmed[1,2], Eric L. Van Nostrand[1,2], Alexander A. Shishkin[1,2,5], Wenhao Jin[1,2], Nancy L. Allbritton[3,4,6] and Gene W. Yeo[1,2] ✉

Genetic screens using pooled CRISPR-based approaches are scalable and inexpensive, but restricted to standard readouts, including survival, proliferation and sortable markers. However, many biologically relevant cell states involve cellular and subcellular changes that are only accessible by microscopic visualization, and are currently impossible to screen with pooled methods. Here we combine pooled CRISPR–Cas9 screening with microraft array technology and high-content imaging to screen image-based phenotypes (CRaft-ID; CRISPR-based microRaft followed by guide RNA identification). By isolating microrafts that contain genetic clones harboring individual guide RNAs (gRNA), we identify RNA-binding proteins (RBPs) that influence the formation of stress granules, the punctate protein–RNA assemblies that form during stress. To automate hit identification, we developed a machine-learning model trained on nuclear morphology to remove unhealthy cells or imaging artifacts. In doing so, we identified and validated previously uncharacterized RBPs that modulate stress granule abundance, highlighting the applicability of our approach to facilitate image-based pooled CRISPR screens.

Pooled genetic knockout screens are widely used by the functional genomics community to identify genes responsible for cellular phenotypes. However, these screens have been limited to bulk selection methods, including growth rate[1], synthetic lethality[2] and reporter-based fluorescent sorting[3,4]. Recently, pooled methods combined with single-cell sequencing[5–8] have allowed for whole-transcriptome quantification following perturbation, enabling multidimensional analyses of molecular pathways associated with genetic alterations. While these methods have dramatically increased the throughput in genetic knockout studies, they cannot assay subcellular phenotypes with the spatiotemporal resolution detected by imaging.

Subcellular phenotypes account for both physiological and pathological changes in cell identity and function, such as transcription factor translocation into the nucleus[9], protein localization to cellular substructures[10] or mislocalization of proteins into disease-associated aggregates[11]. More broadly, high-throughput imaging unbiasedly captures functional and morphological cell states[12] that dictate response to various stimuli[13,14]. However, screening for regulators of these phenotypes is currently limited to arrayed methods that often require expensive robotic platforms. Technologies to integrate pooled screening with cellular and subcellular imaging readouts are critical to improve the throughput of image-based genetic knockout studies. Recently, studies using sequencing in situ with fluorescently labeled nucleotides with pooled CRISPR libraries, in combination with image-based phenotyping, have identified genetic regulators of transcription factor localization[15], cell cycle control in *Escherichia coli*[16] and long noncoding RNA localization[17].

Here we present a new method for pooled CRISPR screens (>12,000 single guide RNAs (sgRNAs)) on microraft arrays[18], followed by automated high-resolution confocal imaging to identify regulators of stress granules, which are cytoplasmic protein aggregates that form during cellular stress. Microraft arrays are an attractive platform to screen bulk-infected cells because thousands of clonal cell colonies (~5–20 cells per colony) can be cultured in isolation from one another after plating cells in limiting dilution[18–20]. Although the microscale cell carriers (rafts) are physically separated from one another on the array, they share a common media reservoir, eliminating artifacts that arise from manipulating hundreds or thousands of cell culture wells individually. And, finally, single microrafts can be removed from the array allowing for extended culture or genomic analyses.

Stress granules are protein–RNA cytoplasmic foci that form transiently during cellular perturbations, such as oxidative stress, heat shock and immune activation[21]. Aberrant stress granule dynamics have been linked to the pathobiology of human diseases, including cancer[22,23] and neurodegeneration[24]. As an illustration, mutations present in amyotrophic lateral sclerosis, a form of neurodegenerative disease, have been shown to alter stress granule dynamics and composition[25–33]. Proteomics approaches have identified proteins that localize to stress granules[33–35]; however, many genes that affect stress granule abundance remain unidentified. Therefore, the identification of genetic modulators that regulate stress granule biology could lead to new disease-relevant therapies.

In this work, we developed CRaft-ID to couple the power of image-based phenotyping of stress granules with an easy-to-use pooled CRISPR screening workflow on microraft arrays. We performed a bulk infection of cells with a gRNA library targeting over 1,000 annotated RBPs (>12,000 sgRNAs), followed by single-cell plating on 20 microraft arrays to screen 119,050 genetic knockout

[1]Department of Cellular and Molecular Medicine, University of California San Diego, La Jolla, CA, USA. [2]Institute for Genomic Medicine and UCSD Stem Cell Program, University of California San Diego, La Jolla, CA, USA. [3]Joint Department of Biomedical Engineering, University of North Carolina at Chapel Hill and North Carolina State University, Chapel Hill and Raleigh, NC, USA. [4]Department of Chemistry, University of North Carolina at Chapel Hill, Chapel Hill, NC, USA. [5]Present address: Eclipse BioInnovations, San Diego, CA, USA. [6]Present address: Department of Bioengineering, University of Washington, Seattle, WA, USA. [7]These authors contributed equally: Emily C. Wheeler, Anthony Q. Vu. ✉e-mail: geneyeo@ucsd.edu

clones for stress granule abundance. Notably, our gRNA library is the same design as those traditionally used for pooled CRISPR screens and requires no library modifications, making this workflow amenable to existing CRISPR gRNA libraries. We performed high-content confocal microscopy and developed machine-learning tools to identify genetic clones with reduced stress granule abundance following CRISPR knockout. Our screen identified and validated six previously known stress granule modulators, along with 17 RBPs that, when depleted, reduce sodium arsenite-induced stress granules in human cells. This work illustrates the power of combining broadly applicable pooled CRISPR methods with microraft-enabled high-content imaging analysis to identify genetic factors that affect subcellular phenotypes.

Results

CRaft-ID screening platform for CRISPR-infected cells. The microraft arrays used in this work consist of 40,000 separable magnetic polystyrene 100-µm square tiles (rafts) as cell-growth surfaces, embedded in a polydimethylsiloxane (PDMS) microwell array substrate. The PDMS barriers between microrafts physically separate the cell colonies, which grow adhered to microrafts within a shared media reservoir. This design allows for standard cell culture and subsequent isolation of individual colonies expanded from single cells. EIF2AK1 is a kinase that initiates stress granule formation by phosphorylating EIF2α in response to oxidative stress induced by sodium arsenite[36]. As a proof-of-concept that variability in stress granule abundance can be reliably measured on these arrays, we pooled cells stably expressing a sgRNA targeting *EIF2AK1* (Fig. 1a,b and Extended Data Fig. 1a) with cells that contain a nontargeting control sgRNA (sg-NTC) on the same array, each expressing a distinguishing nuclear fluorescent marker (Fig. 1c, see Methods). Cells were plated at clonal density (0.3 cells per raft). We observed a doublet rate of 9% by counting the number of wells that contain signal from both fluorescent markers (Extended Data Fig. 1b). Cells were then treated with 500 µM sodium arsenite for an hour to robustly induce stress granules (Extended Data Fig. 1c) that stained positive for the canonical stress granule marker, G3BP1. As expected, mCherry-positive (sg-NTC) colonies contained stress granules, and mCitrine-positive (sg-*EIF2AK1*) colonies did not form stress granules (Fig. 1d,e). We then isolated 56 colonies of each genotype from the array using the respective fluorescent marker to distinguish genotypes. DNA was extracted and prepared into libraries for sequencing using a targeted PCR approach. Of the 112 colonies sequenced, we identified 2 colonies with both guides, and 110 were properly assigned to the predicted genotype (Supplementary Table 1). These results support the utility of the microraft array platform to quantify variability in stress granule formation and accurately assign the proper sgRNA after cell retrieval.

To screen for RBPs that modulate stress granule abundance, we developed a CRISPR–Cas9 gRNA library targeting 1,078 RBPs[37] with 10 sgRNAs targeting each gene (Supplementary Table 2). We included 628 control sgRNAs targeting essential genes and 1,070 nontargeting control sgRNAs (including 12 sgRNAs targeting fluorescent proteins). Of the sgRNAs targeting RBPs, 2,210 are annotated as essential to the survival of HEK293T cells[38]. HEK293T cells were transduced in bulk with the RBP library at low multiplicity of infection (MOI) (0.15 viral particles per cell) and cultured for 7 d to allow sgRNAs targeting lethal genes to deplete from the pool (Fig. 1f). On day 7 postselection, cells were plated at clonal density on the microraft arrays and cultured for 3 d to form small colonies (~5–20 cells per colony) (Fig. 1g). As stress granule quantification required high-resolution, automated confocal imaging that was previously unfeasible on microrafts, we fixed a 1-mm-thick glass slide to the bottom of the microraft arrays using a water-soluble adhesive, which is removed before isolation of the target colonies. This eliminated depth-of-focus variability caused by the soft PDMS material (Extended Data Fig. 1d) and allowed for automated imaging across the entire array.

After quantifying cell abundance with nuclei staining, we determined that ~6,000 colonies formed on each array (15% of wells on the array). To achieve approximately ten times representation of each sgRNA in our library (Extended Data Fig. 1e), we plated a total of 20 arrays, one of which was used as a negative (no stress) control totaling 124,312 plated colonies. As each RBP has ten unique sgRNAs in the library, this results in approximately 100 times coverage per RBP in this experiment. With commercially available microraft arrays, users can scale their screening needs at ~6,000 cell increments with additional arrays. Additional cost associated with PCR-based sequencing is negligible, as the sequencing depth required is low (<100,000 reads per microraft) and standard confocal imaging equipment is readily available.

Automating confocal microscopy for improved resolution and facilitation of high-content screening. To image the microrafts at high resolution, we used automated confocal microscopy to acquire 324 tile scan images in five *z* planes and three color channels across each array (Fig. 2a). We developed computational tools to process these images to isolate individual rafts for analysis (https://github.com/YeoLab/CRaftID). To extract stress granules and nuclei features, we collapsed *z* stacks using the maximum intensity projection of the red (G3BP1) and blue (nuclei) channels. Bright-field images were used to segment each field of view for individual rafts using the defined grid pattern. Individual raft images were then filtered for those containing signal in both the nuclei and G3BP1 channels, and raft images with no cells were discarded. In total, we identified 119,050 colonies from CRISPR-infected, stressed cells, along with 5,262 unstressed control colonies (Fig. 2a).

To remove common aberrations that compromise image quality in high-content screening, we developed a machine-learning tool automating the removal of artifacts before stress granule quantification. A consortium of binary classifiers using convolutional neural networks (CNNs)[39] was trained on images of cells stained for nuclei, making this quality-control step a generalizable approach to other phenotypes screened on this platform. We manually curated a total of 1,477 images of nuclei-stained cells (70% for training, 10% for training validation and 20% for a test set) into five different phenotypic categories: overgrown colonies, debris, lysed cells, autofluorescence and out-of-focus images (Fig. 2b and Extended Data Fig. 2a). Images classified with >99% confidence to any category using a one-versus-all classification approach were eliminated from the dataset, while the remaining images were categorized as healthy and retained in the dataset. Overall multiclass precision was 98%, and the multiclass recall rate was 0.98 when testing this approach on an independent test set of 365 nuclei-stained images (Extended Data Fig. 2b). This filtering approach removed 9% (471 of 5,262) of unstressed colony images and 15% (17,462 of 119,050) of stressed colony images (Fig. 2c).

The remaining 101,588 colony images were quantified for nuclei and stress granule area using a custom pipeline developed in CellProfiler (https://github.com/YeoLab/CRaftID). Images were ranked by the lowest ratio of stress granule to nuclei area and further manually inspected to identify high-confidence colonies containing RBP knockouts that reduce stress granule formation. In total, 101 colonies were isolated from the microraft arrays for targeted-sequencing preparation to identify the infected sgRNA in each colony (Fig. 2d,e).

Identification of sgRNA in selected colonies. To sequence the sgRNA associated with reduced stress granule abundances, we isolated target colonies adhered to microrafts from the array. A motorized microneedle, fitted over the microscope objective, was actuated to pierce the PDMS microarray substrate and dislodge individual

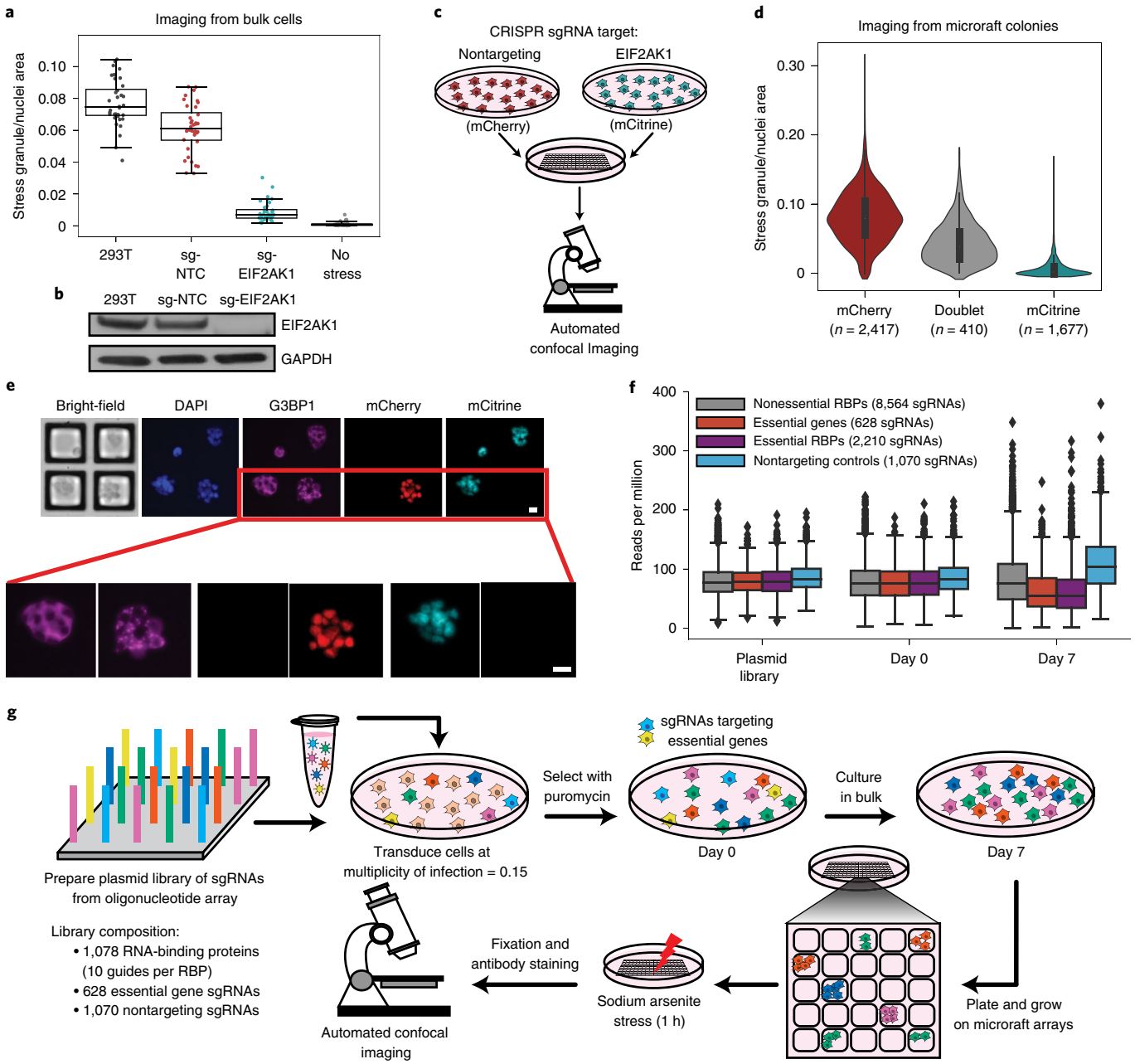

Fig. 1 | Microraft arrays enable the culture and stress granule quantification of thousands of clonal cells. a, Quantification of the ratio of stress granule to nuclei area of cell lines used in the proof-of-concept study, along with an unstressed control. Each data point is one image taken among six different wells plated (6 images per well, total of 36 images per condition). Overlaid box plots represent the interquartile range (IQR; 25th, 50th and 75th percentiles), while whiskers represent 1.5 times the IQR from the 25th (lower) and 75th (upper) percentiles. **b**, Western blot of EIF2AK1 and loading control (GAPDH) in sg-*EIF2AK1*, sg-NTC and uninfected (293T) cells ($n = 1$) **c**, Schematic of pooled experiment used in proof-of-concept study. sg-NTC cells are labeled with mCherry and sg-*EIF2AK1* cells are labeled with mCitrine. Cells were pooled and plated on a microraft array. **d**, Quantification of the ratio of stress granule to nuclei area for all colonies, binned by fluorescent signal. The thick line in the middle of the violin represents the IQR, the middle dot shows the median and the thin lines extend 1.5 times the IQR. **e**, Representative images showing four colonies in the field of view, with zoomed images below. Scale bar, 20 μm. **f**, Relative abundances of sgRNAs in the plasmid library cells at day 0 (after puromycin selection) and day 7. Boxes represent the IQR (25th, 50th and 75th percentiles), while whiskers represent 1.5 times the IQR from the 25th and 75th percentiles. **g**, Cell culture workflow for CRaft-ID. A CRISPR–Cas9 gRNA library was generated from an array of sgRNA oligonucleotides cloned into the lentiCRISPR v2 backbone. HEK293T cells were infected at low multiplicity of infection and cultured in bulk for 7 d after selection, allowing lethal guides (light blue, yellow) to drop out of the pool. Cells were plated on microraft arrays and grown at low density, stressed with sodium arsenite (500 μM), fixed and stained for G3BP1 and nuclei before confocal imaging.

magnetic microrafts from the array. Released microrafts and their cargo were collected with a magnetic wand into a strip tube containing lysis buffer for a targeted two-step PCR with in-line barcodes, followed by high-throughput sequencing (Fig. 3a and Extended Data Fig. 3a). We identified the minimum number of PCR cycles required to amplify enough material for sequencing (22 for PCR1, 10 for PCR2) and size-selected the final library from a 3% agarose gel (Extended Data Fig. 3b–d). Despite isolating genomic DNA from small colonies fixed on the rafts, this method generated a sequencing library for 60% (61) of the picked colonies. The sequencing rate

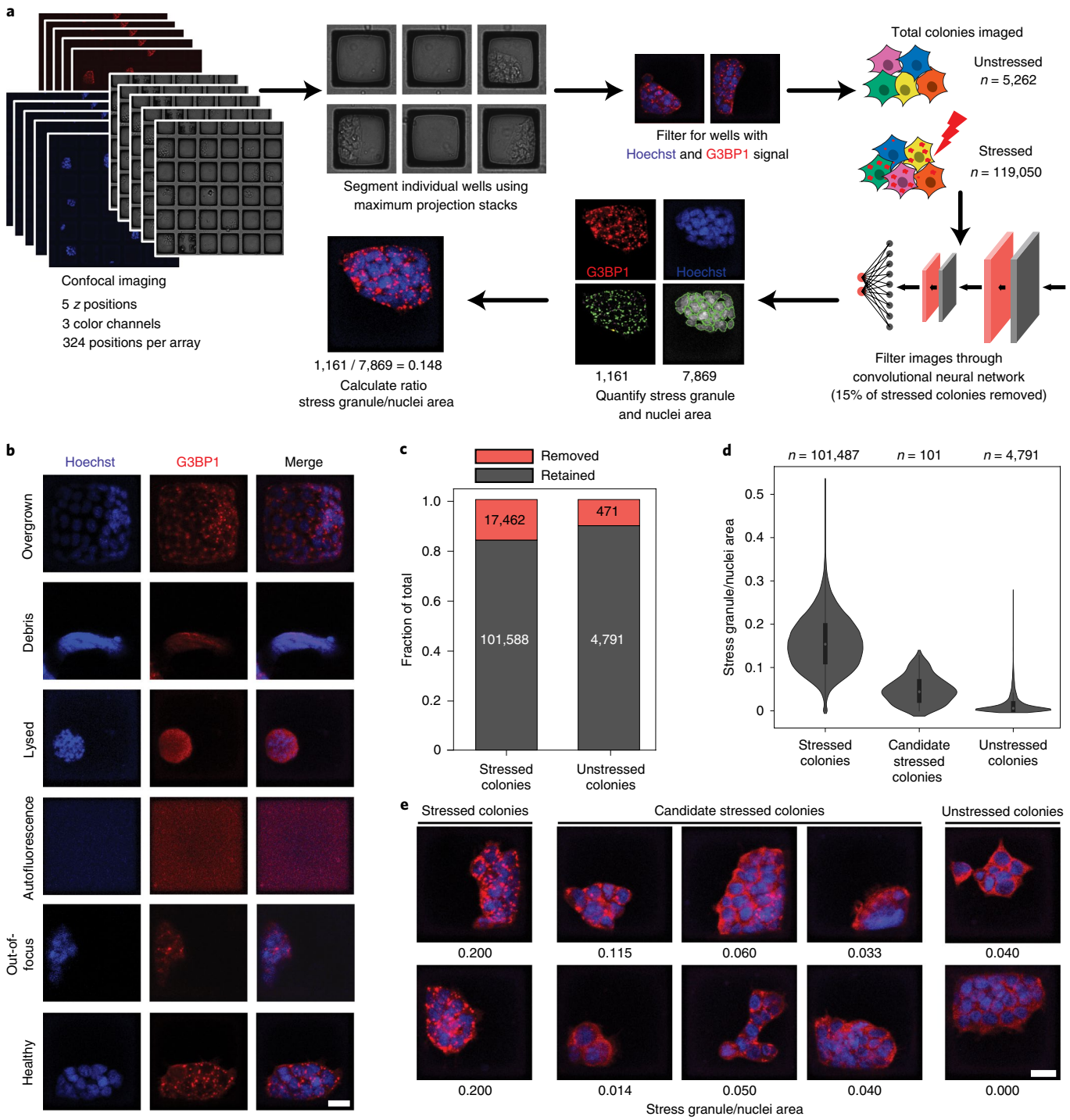

Fig. 2 | Image analysis with CRaft-ID software identifies candidate colonies. a, Schematic of image processing. Confocal microscopy was performed covering each array in 324 fields of view with five *z* stacks and three channels (Hoechst, G3BP1 staining and bright-field). **b**, Example raft images that were discarded using the CNN classification. Raft with healthy cells and acceptable imaging shown at the bottom of the panel. Scale bar, 20 µm. **c**, Fraction of all rafts removed by CNN. A total of 15% of stressed colonies and 9% of unstressed colonies were removed. **d**, Violin plots of stress granule/nuclei area of all healthy raft images. A total of 101 stressed colonies with low stress granule/nuclei area were manually picked as candidates with low stress granule abundance. The thick line in the middle of the violin plot represents the IQR, the white dot shows the median and the thin lines extend 1.5 times the IQR. **e**, Representative images of stressed cells not selected, candidate stressed colonies and unstressed controls. Numbers below each image represent the quantified stress granule/nuclei area. Scale bar, 20 µm.

here is lower than that achieved in the proof-of-concept experiment, which is probably due to the low MOI required for pooled screening. Notably, the population of knockout cells generated for the proof-of-concept experiment was generated with a high MOI and clonally selected to ensure protein depletion, and therefore resulted in a higher sequencing success rate than was observed in the screen. Failure to generate a library could also arise due to incomplete DNA extraction, or to cells peeling off the raft during

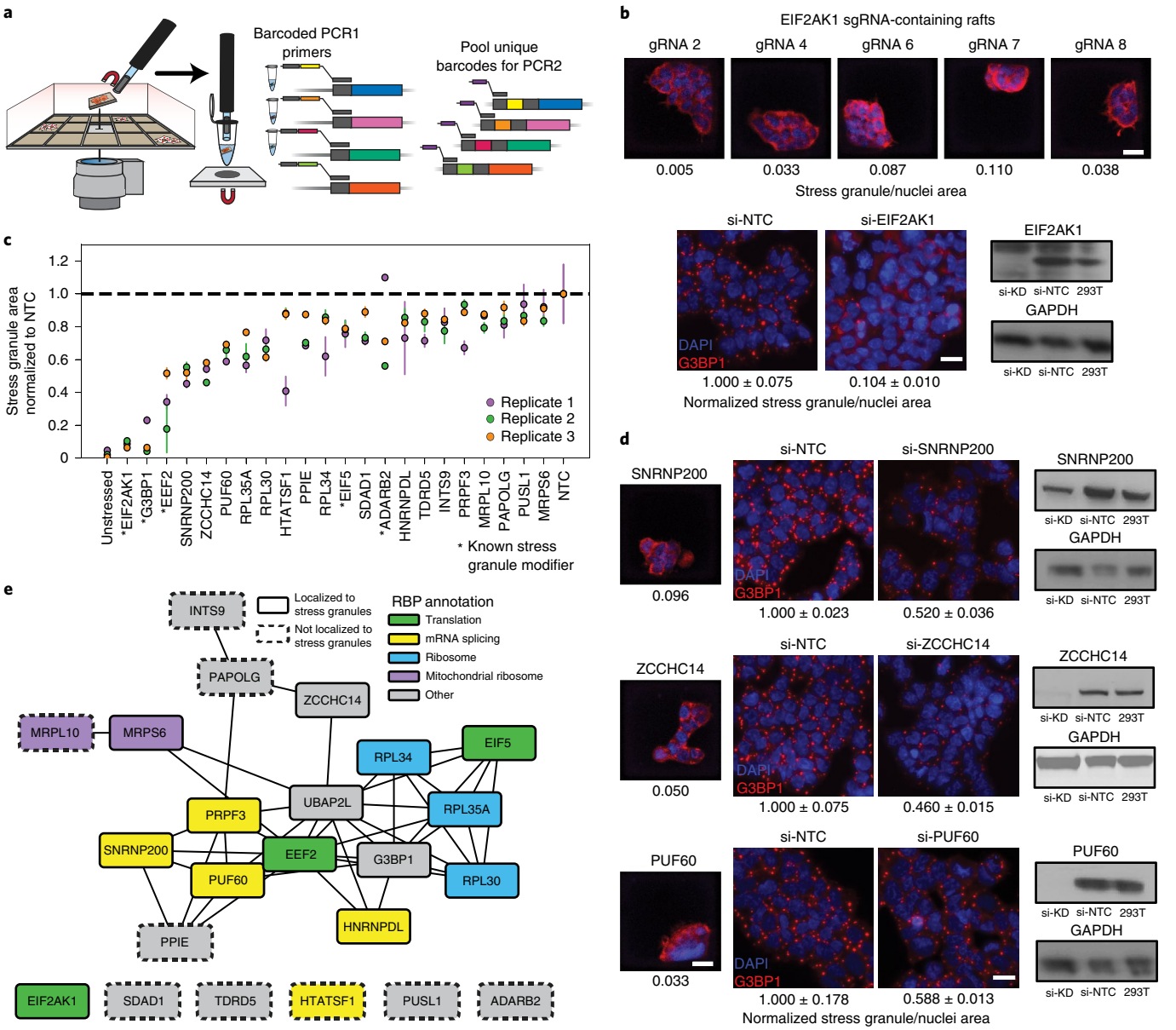

Fig. 3 | sgRNA target identification and validation reveal new stress granule modifiers. a, Diagram of microraft isolation and sgRNA sequencing design. Microrafts are removed from the array using a motorized microneedle fitted over a microscope objective. Dislodged rafts collected with a magnetized wand are placed into individual tubes for DNA extraction and barcoded targeted PCR of the sgRNA insert. **b**, Images of individual, stress-induced microrafts with five different sgRNAs targeting *EIF2AK1*. Scale bar, 20 μm (top). Representative images of G3BP1 antibody staining in sodium arsenite-stressed HEK293T cells after EIF2AK1 depletion by siRNA or nontargeting siRNA control (NTC). Data are mean ±s.d. across $n = 3$ wells per condition (4 images per well). Scale bar, 20 μm (bottom, left). Western blot validation of siRNA-mediated depletion of EIF2AK1 in HEK293T (bottom, right). **c**, siRNA depletion of target RBPs in bulk cells. Stress granule/nuclei area was normalized to the NTC for each experiment. RBPs are ordered on the *x* axis by the lowest normalized stress granule area. RBPs shown here had significant reduction ($P < 0.05$, unpaired two-tailed *t*-test, d.f. = 4, 95% confidence interval) of stress granule area relative to NTC in at least two of the three biological replicates. *Genes previously reported to modify stress granule abundance. Data are mean ±s.d. across $n = 3$ wells per condition (4 images per well). **d**, Validation of SNRNP200, ZCCHC14 and PUF60 (top to bottom). Image of identified microraft colony (left). Representative images of stress-induced G3BP1-positive (red) granule and DAPI (blue) after protein depletion by siRNA in HEK293T or HEK293T-G3BP1-GFP cells (false-colored red for consistency). Scale bar, 20 μm. Quantification below the image is mean stress granule area ±s.d. across $n = 3$ wells per condition (4 images per well) normalized to NTC (middle). Western blot validation of target protein depletion by siRNA (right). KD, knockdown. **e**, Protein–protein interaction network of the 23 RBP targets identified to modulate stress granule abundance. Network visualized in Cytoscape[49]. Protein–protein interactions curated from BioPlex data[48] and recent publications[35].

microraft isolation from the array. Of the successfully sequenced colonies, 49% contained a single gRNA, and 51% contained two or more sgRNAs (Extended Data Fig. 3e and Supplementary Table 3). Importantly, as our sequencing method is able to deconvolute multiple sgRNA colonies, there is no information loss due to doublets, and candidates that occur in multiple rafts are prioritized for independent validation.

Independent validation of candidate stress granule regulators. Reassuringly, the most frequently detected RBP candidate

is our positive control, EIF2AK1, for which we retrieved five different sgRNAs from a total of 12 rafts (Fig. 3b). Images collected from EIF2AK1-identified rafts contain the lowest stress granule area among all sodium arsenite-treated cells in our screen. In addition to EIF2AK1, we detected sgRNAs targeting five other known modulators of stress granule assembly: EEF2 (ref. [40]), G3BP1 (ref. [41]), UBAP2L[33,35], EIF5 (ref. [42]) and ADARB2 (ref. [42]), along with 65 additional candidates.

To independently confirm that candidate RBPs play a role in stress granule abundance, we used a pool of four short interfering RNAs (siRNAs) per target to deplete each RBP in HEK293T cells expressing GFP-tagged G3BP1. We identified a total of 17 RBPs that reduce stress granule abundance by ~10% to ~50% when depleted with siRNAs in at least two of three independent replicate experiments relative to a nontargeting control (Fig. 3c). When possible, we confirmed protein loss by western blot analysis (Fig. 3b,d and Extended Data Fig. 4); however, due to limited antibody availability we could not confirm knockdown for all targets and therefore cannot rule out the possibility that some hits were not validated due to insufficient protein knockdown. In total, 62% (38) of sequenced rafts contained an RBP target that met our validation criteria in siRNA experiments (Extended Data Fig. 3f).

The top three hits not previously known to regulate stress granules were SNRNP200, ZCCHC14 and PUF60, each of which reduced stress granule abundance by ~50% when depleted with siRNAs (Fig. 3d). Interestingly, loss-of-function alterations in each of these proteins have been implicated in neurological diseases. PUF60 loss-of-function is associated with microcephaly and intellectual disability[43], SNRNP200 is lost in patients with retinitis pigmentosa[44] and ZCCHC14 mutations are found in patients with cerebral small vessel disease and autism spectrum disorder[45,46]. While no direct link has been made between these diseases and stress granule biology, our results raise the possibility that cytoplasmic granules may play a role, given their strong association with neurodegenerative disease.

To determine whether the identified factors influence recruitment of other known stress granule components, we co-stained cells from siRNA knockdown experiments for UBAP2L and quantified the abundance of UBAP2L-positive granules. We found that 12 of the 22 candidates tested contained a significant reduction ($P < 0.05$) in UBAP2L-positive granules in at least three of four replicate experiments (Extended Data Fig. 5a,b). Interestingly, we observed an abundance of UBAP2L-positive granules in cells depleted for G3BP1. This supports a recently published model of distinct UBAP2L-positive stress granule cores that act independently of G3BP1 and can nucleate G3BP1-positive stress granule assemblies[47].

To reveal the direct, or indirect, role that these candidate RBPs have in regulating stress granule abundance, we generated a protein–protein interaction (PPI) network by curating the interactomes of UBAP2L and G3BP1 (ref. [35]), as well as the BioPlex project of experimentally validated and predicted PPIs[48]. Many of the modulators identified in this work localize to stress granules (Fig. 3e, solid outlines) and interact with G3BP1. Importantly, some RBPs do not colocalize in stress granules or interact with other stress granule modulators identified in this screen (Fig. 3e, dashed outlines). These RBPs represent regulatory nodes of stress granule assembly that exist independently from direct granule formation.

Discussion

The CRaft-ID screening platform presented here represents an advance and expansion of the application of pooled screening approaches to encompass cellular and subcellular phenotypic readouts. This method is widely accessible as it employs standard cell culture practices, CRISPR libraries, off-the-shelf confocal imaging techniques and PCR-based DNA sequencing. In this work, we screened for genetic modulators of stress granule abundance in human cells by analyzing ~120,000 lentiCRISPR-infected cell colonies. This resulted in the identification of both known and unexpected RBPs that regulate stress granule assembly.

Microraft arrays behave like standard cell culture dishes, and therefore can accommodate a variety of cell types, including stem cells[19] and cells derived from differentiation protocols. However, this method may not be easily amenable to nondividing cells plated directly onto the array. CRaft-ID is best suited to screen for regulators of rare phenotypes among a population of genetic knockouts, as individual microrafts must be isolated and PCR amplified to determine the infected sgRNA. In instances where a phenotype is affected by a large fraction of sgRNAs, an alternative strategy is to isolate many microrafts into a single tube and prepare one library to sequence all sgRNAs in the combined pool. As manual isolation of microrafts takes ~2 min per raft, it is feasible to pick hundreds of rafts.

Two alternative approaches have been used to perform imaging-based pooled genetic screening with varying degrees of throughput and resolution. The first was optimized for detection of high-resolution phenotypes (RNA localization), albeit low throughput (54 genes targeted, 30,000 cells imaged)[17], while the second performed high-throughput measurement (963 genes targeted, 3 million cells imaged) of low-resolution phenotypes (nuclear/cytoplasmic localization)[15]. The CRaft-ID platform, by comparison is intermediate with regards to throughput (1,078 genes targeted, 120,000 colonies imaged) and resolution of phenotype (cytoplasmic protein–RNA puncta). In contrast to these methods, which use sequencing-by-synthesis of fluorescently labeled nucleotides, CRaft-ID uses traditional PCR-based sequencing to identify the infected sgRNA. While the image-based sequencing approaches have the benefit of identifying the sgRNA barcode present in all screened cells, they require a customized microscope setup and data analysis engine. Additionally, CRaft-ID is a platform that is compatible with live-cell recovery upon phenotypic selection. In our work, sodium arsenite treatment is lethal to cells after washout, and stress granule formation is transient; therefore, colonies were fixed to preserve their morphology before imaging. However, in experiments where perturbation is nonlethal to cells, imaging can be performed on live colonies to capture dynamic localization patterns of endogenously tagged proteins and cell morphology, followed by live-cell colony isolation from the array for further cell-based studies[18].

In conclusion, CRaft-ID expands the utility of CRISPR screening to high-content imaging, allowing for the interrogation of genetic modulators of subcellular and cell-morphological phenotypes that have previously been inaccessible with bulk-infection methods. We have shown here that CRaft-ID can robustly identify both previously described and newly validated modulators of stress granule abundance, providing insight into stress granule biology. This platform is accessible and flexible to countless imaging-based phenotypes, creating a notable advancement in the field of functional genomics screening.

Online content

Any methods, additional references, Nature Research reporting summaries, source data, extended data, supplementary information, acknowledgements, peer review information; details of author contributions and competing interests; and statements of data and code availability are available at https://doi.org/10.1038/s41592-020-0826-8.

Received: 30 October 2019; Accepted: 6 April 2020;
Published online: 11 May 2020

References

1. Shalem, O. et al. Genome-scale CRISPR–cas9 knockout screening in human cells. *Science* **343**, 84–87 (2014).

2. Blomen, V. A. et al. Gene essentiality and synthetic lethality in haploid human cells. *Science* **350**, 1092–1096 (2015).
3. DeJesus, R. et al. Functional CRISPR screening identifies the ufmylation pathway as a regulator of SQSTM1/p62. *eLife* **5**, e17290 (2016).
4. Parnas, O. et al. A genome-wide CRISPR screen in primary immune cells to dissect regulatory networks. *Cell* **162**, 675–686 (2015).
5. Jaitin, D. A. et al. Dissecting immune circuits by linking CRISPR-pooled screens with single-cell RNA-Seq. *Cell* **167**, 1883–1896.e15 (2016).
6. Adamson, B. et al. A multiplexed single-cell CRISPR screening platform enables systematic dissection of the unfolded protein response. *Cell* **167**, 1867–1882.e21 (2016).
7. Dixit, A. et al. Perturb-Seq: dissecting molecular circuits with scalable single-cell RNA profiling of pooled genetic screens. *Cell* **167**, 1853–1866.e17 (2016).
8. Datlinger, P. et al. Pooled CRISPR screening with single-cell transcriptome readout. *Nat. Methods* **14**, 297–301 (2017).
9. Link, W. et al. Chemical interrogation of FOXO3a nuclear translocation identifies potent and selective inhibitors of phosphoinositide 3-kinases. *J. Biol. Chem.* **284**, 28392–28400 (2009).
10. de Groot, R., Luthi, J., Lindsay, H., Holtackers, R. & Pelkmans, L. Large-scale image-based profiling of single-cell phenotypes in arrayed CRISPR-Cas9 gene perturbation screens. *Mol. Syst. Biol.* **14**, e8064 (2018).
11. Maharana, S. et al. RNA buffers the phase separation behavior of prion-like RNA binding proteins. *Science* **360**, 918–921 (2018).
12. Caicedo, J. C., Singh, S. & Carpenter, A. E. Applications in image-based profiling of perturbations. *Curr. Opin. Biotechnol.* **39**, 134–142 (2016).
13. Kiger, A. A. et al. A functional genomic analysis of cell morphology using RNA interference. *J. Biol.* **2**, 27 (2003).
14. Liu, T., Sims, D. & Baum, B. Parallel RNAi screens across different cell lines identify generic and cell type-specific regulators of actin organization and cell morphology. *Genome Biol.* **10**, R26 (2009).
15. Feldman, D. et al. Optical pooled screens in human cells. *Cell* **179**, 787–799. e17 (2019).
16. Camsund, D. et al. Time-resolved imaging-based CRISPRi screening. *Nat. Methods* **17**, 86–92 (2020).
17. Wang, C., Lu, T., Emanuel, G., Babcock, H. P. & Zhuang, X. Imaging-based pooled CRISPR screening reveals regulators of lncRNA localization. *Proc. Natl Acad. Sci. USA* **116**, 10842–10851 (2019).
18. Wang, Y. et al. Micromolded arrays for separation of adherent cells. *Lab Chip* **10**, 2917–2924 (2010).
19. DiSalvo, M., Smiddy, N. M. & Allbritton, N. L. Automated sensing and splitting of stem cell colonies on microraft arrays. *APL Bioeng.* **3**, 036106 (2019).
20. Gach, P. C., Wang, Y., Phillips, C., Sims, C. E. & Allbritton, N. L. Isolation and manipulation of living adherent cells by micromolded magnetic rafts. *Biomicrofluidics* **5**, 032002 (2011).
21. Kedersha, N. & Anderson, P. Mammalian stress granules and processing bodies. *Methods Enzymol.* **431**, 61–81 (2007).
22. Anderson, P., Kedersha, N. & Ivanov, P. Stress granules, P-bodies and cancer. *Biochim. Biophys. Acta* **1849**, 861–870 (2015).
23. Grabocka, E. & Bar-Sagi, D. Mutant KRAS enhances tumor cell fitness by upregulating stress granules. *Cell* **167**, 1803–1813.e12 (2016).
24. Wolozin, B. & Ivanov, P. Stress granules and neurodegeneration. *Nat. Rev. Neurosci.* **20**, 649–666 (2019).
25. Murakami, T. et al. ALS/FTD mutation-induced phase transition of FUS liquid droplets and reversible hydrogels into irreversible hydrogels impairs RNP granule function. *Neuron* **88**, 678–690 (2015).
26. Patel, A. et al. A liquid-to-solid phase transition of the ALS protein FUS accelerated by disease mutation. *Cell* **162**, 1066–1077 (2015).
27. Boeynaems, S. et al. *Drosophila* screen connects nuclear transport genes to DPR pathology in c9ALS/FTD. *Sci. Rep.* **6**, 20877 (2016).
28. Lee, K. H. et al. C9orf72 dipeptide repeats impair the assembly, dynamics, and function of membrane-less organelles. *Cell* **167**, 774–788.e17 (2016).
29. Lin, Y. et al. Toxic PR poly-dipeptides encoded by the C9orf72 repeat expansion target LC domain polymers. *Cell* **167**, 789–802.e12 (2016).
30. Martinez, F. J. et al. Protein-RNA networks regulated by normal and ALS-associated mutant HNRNPA2B1 in the nervous system. *Neuron* **92**, 780–795 (2016).
31. Mackenzie, I. R. et al. TIA1 mutations in amyotrophic lateral sclerosis and frontotemporal dementia promote phase separation and alter stress granule dynamics. *Neuron* **95**, 808–816.e9 (2017).
32. Fang, M. Y. et al. Small-molecule modulation of TDP-43 recruitment to stress granules prevents persistent TDP-43 accumulation in ALS/FTD. *Neuron* **103**, 802–819.e11 (2019).
33. Markmiller, S. et al. Context-dependent and disease-specific diversity in protein interactions within stress granules. *Cell* **172**, 590–604.e13 (2018).
34. Jain, S. et al. ATPase-modulated stress granules contain a diverse proteome and substructure. *Cell* **164**, 487–498 (2016).
35. Youn, J. Y. et al. High-density proximity mapping reveals the subcellular organization of mRNS-associated granules and bodies. *Mol. Cell* **69**, 517–532.e11 (2018).
36. McEwen, E. et al. Heme-regulated inhibitor kinase-mediated phosphorylation of eukaryotic translation initiation factor 2 inhibits translation, induces stress granule formation, and mediates survival upon arsenite exposure. *J. Biol. Chem.* **280**, 16925–16933 (2005).
37. Gerstberger, S., Hafner, M. & Tuschl, T. A census of human RNA-binding proteins. *Nat. Rev. Genet.* **15**, 829–845 (2014).
38. Hart, T. et al. Evaluation and design of genome-wide CRISPR/SpCas9 knockout screens. *G3* **7**, 2719–2727 (2017).
39. LeCun, Y., Bengio, Y. & Hinton, G. Deep learning. *Nature* **521**, 436–444 (2015).
40. Schneider-Poetsch, T. et al. Inhibition of eukaryotic translation elongation by cycloheximide and lactimidomycin. *Nat. Chem. Biol.* **6**, 209–217 (2010).
41. Tourriere, H. et al. The RasGAP-associated endoribonuclease G3BP assembles stress granules. *J. Cell Biol.* **160**, 823–831 (2003).
42. Ohn, T., Kedersha, N., Hickman, T., Tisdale, S. & Anderson, P. A functional RNAi screen links O-GlcNAc modification of ribosomal proteins to stress granule and processing body assembly. *Nat. Cell Biol.* **10**, 1224–1231 (2008).
43. Low, K. J. et al. PUF60 variants cause a syndrome of ID, short stature, microcephaly, coloboma, craniofacial, cardiac, renal and spinal features. *Eur. J. Hum. Genet* **25**, 552–559 (2017).
44. Zhang, X. et al. Contribution of SNRNP200 sequence variations to retinitis pigmentosa. *Eye* **27**, 1204–1213 (2013).
45. Handrigan, G. R. et al. Deletions in 16q24.2 are associated with autism spectrum disorder, intellectual disability and congenital renal malformation. *J. Med. Genet.* **50**, 163–173 (2013).
46. Chung, J. et al. Genome-wide association study of cerebral small vessel disease reveals established and novel loci. *Brain* **142**, 3176–3189 (2019).
47. Cirillo, L. et al. UBAP2L forms distinct cores that act in nucleating stress granules upstream of G3BP1. *Curr. Biol.* **30**, 698–707.e96 (2020).
48. Huttlin, E. L. et al. The bioplex network: a systematic exploration of the human interactome. *Cell* **162**, 425–440 (2015).
49. Shannon, P. et al. Cytoscape: a software environment for integrated models of biomolecular interaction networks. *Genome Res.* **13**, 2498–2504 (2003).

Publisher's note Springer Nature remains neutral with regard to jurisdictional claims in published maps and institutional affiliations.

© The Author(s), under exclusive licence to Springer Nature America, Inc. 2020

Methods

Generating mCitrine and mCherry fluorescently labeled HEK293T cells. PiggyBAC shuttle vectors expressing mCitrine or mCherry[50] were stably integrated via transient transfection. Plasmids were delivered by transfecting 70% confluent HEK293T in a 6-well plate using 2 µg PiggyBAC shuttle vector, 0.5 µg Super PiggyBAC transposase[50] and 12 µl of Lipofectamine 2000. Medium was replaced 24 h after transfection with DMEM supplemented with 10% fetal bovine serum (FBS).

Generating HEK293T cells stably expressing EIF2AK1 or NTC sgRNA. sgRNAs targeting *EIF2AK1* and a nontargeting control were cloned into the LentiCRISPR v2 backbone[51]. sgRNAs and backbone were digested with BsmBI restriction digest and ligated with T4 DNA ligase. Complete plasmids were confirmed with Sanger sequencing.

sgRNA *EIF2AK1*: TTTAACACCTGGATTTGTGC
sgRNA NTC: TCCCAAGGGTTTAAGTCGGG

Lentiviral particles were packaged in a 10-cm plate by transfecting HEK293xT at 70% confluency with 10 µg of complete lentiCRISPR v2 plasmid, 5 µg of PMD2.G, 7.5 µg of psPAX2, 45 µl of P3000 reagent and 45 µl of Lipofectamine 3000. Medium was replaced the next day with 7 ml DMEM supplemented with 10% FBS. At 72 h posttransfection, medium containing lentivirus was collected, centrifuged at 400*g* for 5 min and 2 ml of supernatant was used to transduce a 6-well plate of fluorescently labeled HEK293T cells. After 48 h, transduced cells were treated with 2 µg ml^{-1} puromycin for 3 d to select for infected cells. To identify cells edited by sgRNA targeting *EIF2AK1*, mCitrine-positive cells were sorted by single-cell fluorescence-activated cell sorting (FACS) into a 96-well plate. Cells were grown for 7–9 d before being re-plated onto two replicate 96-well plates. For the plate used to phenotype cell clones, cells were stressed and stained as described in Cell stress treatment and antibody staining. The hit clone from the replicate well was expanded for the pilot experiment and protein knockout was validated with western blotting.

Microraft array microfabrication. Microraft array microfabrication followed previously reported techniques[20,52]. The elastomeric microarray substrates were fabricated via soft-lithographic molding of PDMS microwells from photoresist-negative templates. Specifically, a 300-µm PDMS precursor layer was sandwiched between an octyltrichlorosilane-treated template and a 1-mm-thick glass slide cleaned with acetone and coated with 30 kDa poly(acrylic acid). Solid PDMS microwells were formed by curing the sandwich for 40 min at 95 °C and demolding the template. The glass-laminated PDMS microwell substrate was dip-coated in poly(styrene-co-acrylic acid) with iron oxide nanoparticles in γ-butyrolactone solvent. As the substrate was retracted from the solution, beads of polymer were formed within each PDMS microwell via discontinuous dewetting of the solution. The polymer microrafts were solidified overnight at 95 °C. Injection-molded polystyrene media chambers were cleaned by a 1-h sonication and overnight incubation in detergent (Alcanox), followed by isopropanol and water rinses. The media chambers were dried and then attached to the microraft arrays using PDMS that was cured for 3 h at 70 °C. The glass laminate was retained on the microraft array during confocal microscopy imaging. Microraft arrays are commercially available through Cell Microsystems.

Microraft cell culture. Microraft arrays were plasma treated (Harrick Plasma) for 5 min and sterilized using a 30-min incubation in 75% ethanol. After three serial 5-min rinses in 1× PBS to remove traces of ethanol, the microraft arrays were coated in 0.001% w/v poly-D-lysine (PDL) for 1 h at 37 °C. The PDL-coated array was washed twice with 1× PBS and stored in cell-growth media until cell culture. For the pilot experiment, mCitrine-positive (with sgRNA targeting EIF2AK1) and mCherry-positive (with nontargeting sgRNA) were dissociated and passed through a 40-µm mesh filter to remove clumps. Cells were then combined at a 1:1 ratio and a total of 1.2×10^4 cells were plated on the array in 1 ml DMEM supplemented with 10% FBS and 1% PenStrep (Gibco, catalog no. 15140122). For the screen, dissociated CRISPR-infected HEK293T cells were filtered through a 40-µm mesh filter to remove clumps and 1.2×10^4 cells were plated onto each array in 1 ml DMEM with 10% FBS and 1% PenStrep. Arrays were spun at 400*g* for 4 min in a swinging-bucket centrifuge to settle cells onto the microraft and stored at 37 °C, 5% CO_2. After 24 h, 2 ml of medium was added to each microarray.

Cell stress treatment and antibody staining. After 72 h in culture on the microraft, cells were treated with 500 µM sodium arsenite in DMEM supplemented with 5% FBS for 1 h at 37 °C. To fix the cells, 12% paraformaldehyde (PFA) was added to a final concentration of 4% PFA and incubated for 15 min at room temperature. Three washes with wash buffer (0.01% Triton-X in 1× PBS) were performed to remove the PFA. Blocking and cell permeabilization were performed with 1-h incubation in 0.1% Triton-X (SigmaAldrich, catalog no. X100) and 5% goat serum (SigmaAldrich, catalog no. G9023) diluted in 1× PBS. The cells were then washed with wash buffer and incubated in the primary antibody solution overnight at 4 °C (wash buffer with 5% goat serum, 1:1,000 rabbit anti-G3BP1 (MBL, catalog no. RN048PW, RRID:AB_10794608)). Samples were washed three times in wash buffer before being incubated in secondary antibody solution (wash buffer with 5% goat serum, 1:1,000 Alexa Fluor 555 goat anti-rabbit (Invitrogen, catalog no. A21429, RRID:AB_141761) or 1:1,000 Alexa Fluor 633 goat anti-rabbit (Invitrogen, catalog no. A21070, RRID:AB_2535731)) for 1 h at room temperature. Cells were then washed three times with wash buffer and incubated with Hoechst 33342 (Thermo Scientific, catalog no. 62249) diluted to 1 µg ml^{-1} in wash buffer for 30 min. Microrafts were stored in 1× PBS containing 1% PenStrep for imaging and colony isolation.

Confocal imaging of microraft array. The microraft array plated with fluorescently labeled sg-*EIF2AK1* and sg-NTC CRISPR-infected 293T cells was imaged using a Crest X-Light V2 L-FOV spinning disk confocal with a Lumencor Celesta laser engine and mounted on a Nikon Eclipse Ti2 microscope. Images were acquired using a Hamamatsu ORCA Fusion sCMOS camera. The system was operated with NIS Elements High Content software (Nikon). A ×10 objective (0.45 numerical aperture) was used to collect a 42-µm-thick stack with seven *z* slices for each of the 324 views acquired to capture the entire raft. The 405 nm, 520 nm, 546 nm and 638 nm lines of the Celesta were used to capture 4,6-diamidino-2-phenylindole (DAPI), mCitrine, mCherry and Alexa647/Cy5, respectively. A Semrock penta-primary dichroic and 450/40, 535/30, 595/31 and 694/72 band-pass emission filters were used to separate excitation and emission light.

To image fixed RBP CRISPR-infected cells on microrafts for the screen, laser scanning confocal microscopy was performed using an Olympus FluoView 3000 microscope operated with Olympus software. An Olympus ×10 objective (Olympus, catalog no. UPLSAPO 10) with 0.4 numerical aperture and 3.1 mm working distance was used with a ×1 digital zoom and 0.62 µm per pixel digital resolution. Images were acquired in a 35 µm focal range, with five optical slices with 7 µm between slices, through colonies adhered to the microraft surface. An 18 × 18 paneling of field of views was used to scan a 1 inch^2 microraft array with 14%, or 180 µm, overlap between adjacent images. Excitation/emission of Hoechst 33342 and Alexa Fluor 555 were performed simultaneously with combined 405- and 561-nm lasers and a multispectral detector set for wavelengths of 430–470 nm and 615–715 nm, respectively. A confocal aperture of 118 µm was used for all imaging. Sample tilt correction was utilized.

Image processing. A total of 324 images containing three channels and five slices per channel were collected per microraft array. The five slices were merged with the maximum intensity projection function in FIJI and saved as a single image per channel. Bright-field images were used to segment each image on individual microrafts for further analysis using custom Python scripts (https://github.com/YeoLab/CRaftID). Individual rafts were filtered based on Hoechst 33342 and Alexa Fluor 555 signal to select rafts that contained cells and remove empty wells.

CRISPR plasmid library preparation. A comprehensive list of sgRNA sequences projected to efficiently direct Cas9 cleavage at their target sites was generated using the sequence model using CRISPR-FOCUS[53] and ordered as a pool of equal molar oligonucleotides (Supplementary Table 2). The lentiCRISPR RBP plasmid library was cloned using previously reported methods[1]. Briefly, the lentiCRISPR v2 backbone[51] was digested using BsmBI restriction sites and sgRNA oligonucleotide inserts were PCR amplified and Gibson assembled using 36 parallel electroporations to maintain a ×300 library complexity. Transformations were spread on 14 carbenicillin selection agar plates (24.5 cm × 24.5 cm). Colonies were grown for 16–18 h at 32 °C. The next day, colonies were scraped off the plates and the cell pellet was maxiprepped (~0.9 g of cells per column). The plasmid library was stored at −20 °C.

CRISPR library virus preparation. HEK293xT cells were seeded on twelve 15-cm plates cells at 40% confluency the day before transfection. One hour before transfection the media was removed and replaced with 8 ml of prewarmed OptiMEM. Transfections were performed using 62.5 µl of Lipofectamine 2000, 125 µl of Plus reagent, 12.5 µg of lentiCRISPR plasmid library, 6.25 µg of pMD2.G and 9.375 µg of psPAX2. Media was changed 6 h after transfection to DMEM supplemented with 10% FBS. After 48 h, the supernatant was filtered through a 0.45-µm low protein binding membrane. The virus was then ultracentrifuged at 24,000 r.p.m. for 2 h at 4 °C and resuspended overnight at 4 °C in PBS. Virus aliquots were stored at −80 °C.

Multiplicity of infection. The volume of virus to achieve a MOI of 0.15 was determined by titrating virus in each well of a 6-well plate (tested volumes ranged from 0.5 µl to 6 µl per well). A total of 7×10^5 cells per well of a 6-well plate were transduced in medium supplemented with 8 µg ml^{-1} polybrene for 24 h. Media (without polybrene) was then replaced and half the cells were split into replicate wells, one of which was treated with 2 µg ml^{-1} puromycin. Cells were counted after 3–4 d and MOI was determined by the volume of virus that allows 15% of the cells to survive.

Viral infection of 293T cells with RBP CRISPR–Cas9 library. HEK293T cells (4.2×10^6 cells per 10-cm plate) were seeded on four plates. Lentivirus (18 µl per plate) was added the next day in medium supplemented with 8 µg ml^{-1} polybrene. Lentivirus was removed 24 h later, and transduced cells were treated with 2 µg ml^{-1} puromycin for 3 d. Plates were then combined and seeded onto microrafts.

Classification of healthy colony images. To infer the classification of an image as a healthy colony or as one of several unwanted classes of colony images, it was fed through a series of binary classifiers with CNNs. The models were trained on a manually curated set of 1,477 nuclei-stained images using the Keras-Tensorflow framework running on P6000 GPU instances on Paperspace. During inference, if any classifier in the model gave positive classification to an image above a 99% confidence threshold, the image was classified as such. If none of the classifiers positively called the image, the image was retained for quantification of stress granule abundance.

Stress granule image segmentation and quantification. Nuclei and stress granule images were segmented and quantified using a custom pipeline developed in CellProfiler (v.3.0.0, available at https://github.com/YeoLab/CRaftID). Nuclei were identified in the DAPI channel using an object diameter threshold of 9–80 pixel units. To eliminate autofluorescent signal from artifacts detected outside the cell boundaries, a cell body mask was generated by overlaying the granule channel (G3BP1 or UBAP2L) and propagating a trace from nuclei to the edge of the cytoplasmic protein fluorescent signal. Punctate structures in cell bodies were image processed to enhance speckles with a maximum feature size of 6 pixel units. Stress granules were identified from the enhanced image using an object diameter of 2–10 pixel units. Total stress granule and nuclei area were measured from each image.

Microraft cell isolation. Microrafts containing hit cells were isolated from the microraft array using a motorized microneedle device and previously reported methods[20,54]. Before isolation, the glass laminate was removed from the microraft array using an overnight incubation in water to dissolve the poly(acrylic acid) adhesive. The position of target rafts was calculated in micrometer distances relative to the upper-left corner of the array using image-processing scripts available on GitHub (https://github.com/YeoLab/CRaftID). The motorized microneedle device and microraft array were placed on an Olympus IX81 microscope. A custom software graphical user interface was used to automatically position and actuate the microneedle to puncture the elastomeric PDMS array substrate, thus dislodging the target microraft and its cellular cargo. This method can be adopted to any motorized stage using the coordinates calculated for each target microraft and manual calibration of the microneedle device (~5 min setup per picking session). A hand-manipulated magnetic wand was utilized to transfer the floating microraft into 6 µl of QuickExtract (Lucigen, catalog no. QE09050) buffer in a strip tube. The time required to isolate and collect individual microrafts was approximately 2 min. (Microneedles and the motorized device are commercially available through Cell Microsystems.)

Guide identification of target wells. Isolated rafts were stored at −20 °C in QuickExtract buffer until library preparation. Samples were thawed and DNA was isolated following the manufacturer's protocol: 15 s vortex, 65 °C for 6 min, 15 s vortex, 98 °C for 2 min. All PCR reactions were carried out with Q5 High-Fidelity DNA polymerase (NEB, catalog no. M0492L). A first round containing 22 PCR cycles was performed using indexed PCR primers targeting the common regions flanking the CRISPR guides that contain a handle for sequencing barcodes to bind in a subsequent reaction. Four individual reactions with unique index sequences from the first PCR were combined and purified with a Qiagen PCR purification kit to generate the template for a second round of PCR with ten cycles. A second round of PCR was performed using the purified template and Illumina sequencing primers to generate a sequencing library. Gel extraction was used to specifically isolate the desired product for sequencing (260 base pairs (bp)). Libraries were sequenced on an Illumina HiSeq 4000 SE75 (rafts from full screen) or Illumina MiSeq SE150 (rafts from pilot experiment). For more details, see the Supplementary Experimental Protocol.

(NNNNNN is reserved for a unique, 6-bp index sequence).

PCR1 Fwd: CCTACACGACGCTCTTCCGATCT**NNNNNN**TTCTTG-TGGAAAGGACGAAACACC

PCR1 Rev: GTTCAGACGTGTGCTCTTCCGATCTCCACTTTTTCAA-GTTGATAACGGACTAGCC

PCR2 Fwd: AATGATACGGCGACCACCGAGATCTACACTATAGCCTAC-ACTCTTTCCCTACACGACGCTCTTCCGATCT

PCR2 Rev: CAAGCAGAAGACGGCATACGAGATCGAGTAATGTGACTG-GAGTTCAGACGTGTGCTCTTCCGATC

Bulk CRISPR gRNA library preparation. *DNA preparation.* DNA libraries were prepared using a targeted-enrichment approach. Genomic DNA was extracted from pellets of 4 million cells using DNeasy Blood & Tissue kit (Qiagen, catalog no. 69504) eluted in 130 µl, with typical yields of 150 ng µl^{-1}. Genomic DNA samples were sonicated to ~1,000 bp by Bioruptor. Average fragment size was determined with genomic DNA ScreenTapes on the Agilent Tapestation (Agilent, catalog no. 5067-5365).

Probe generation. To selectively enrich sgRNA-containing regions in the genomic DNA, we generated two antisense probes by PCR amplification of a ~500-nucleotide constant region flanking the sgRNA sequence. Corresponding 592-nucelotide and 574-nucleotide biotinylated RNA probes were generated using HiScribe T7 High Yield RNA Synthesis Kit (NEB, catalog no. E2040S) with bio-CTP (Thermo Scientific, catalog no. 19519016) and bio-UTP (Sigma/Roche, catalog no. 11388908910) nucleotides.

PCR Primer set 1:

Fwd: GGGATATTCACCATTATCGTTTCAGACC

Rev: GGATTCTAATACGACTCACTATAGGGTGTTTCGTCCTT TCCACAAGA

PCR Primer set 2:

Fwd: GGTGTATCTTCTTCTGGCGGTTC

Rev: GGATTCTAATACGACTCACTATAGGGCAAGTTAAAAT-AAGGCTAGTCCGTTATCA

Probe capture. Dithiothreitol (DTT, 1% of 1 M) was added to genomic DNA for a final concentration of 10 mM. Concentration of probes was determined for each sample as 10% of the total DNA yield (in µg), diluted in water to a final volume of 10 µl. Samples were placed in a preheated thermomixer set at 95 °C with interval mixing (1,200 r.p.m., 30 s on/1 min off). Immediately after adding the samples, the temperature was changed to 65 °C to begin cooling. When cooled to 65 °C, 10 µl of probes was added, followed by 73.5 µl of 3× hybridization buffer (75 mM Tris, 15 mM EDTA, 1.2 M LiCl, 3 M urea, 0.3% NP-40, 0.3% SDS, 0.3% DOC). Incubation was performed with interval mixing as follows: 65 °C for 5 min, 64 °C for 5 min, 63 °C for 5 min, 62 °C for 5 min, 61 °C for 150 min.

Streptavidin capture. Streptavidin beads (30 µl, Invitrogen, catalog no. 11205D) per 1 µg of probes was used for each sample, washed with 500 µl of 1× hybridization buffer and resuspended in 20 µl of 1× hybridization buffer. Following probe capture, 14 µl of beads (75%) was added to each sample and incubated for 15 min at 62 °C with interval mixing. Supernatant was removed and transferred back into the tube with the remaining 25% of the beads for a second round of hybridization (62 °C with interval mixing for 15 min). Meanwhile, the collected beads (75%, on-magnet) were resuspended in 200 µl of prewarmed 1× hybridization buffer and incubated for 5 min at 37 °C. Supernatant was discarded and tubes were kept on ice. Following the second 15-min incubation, supernatant was discarded from the tube containing the remaining 25% of beads and the beads were resuspended in 200 µl of prewarmed 1× hybridization buffer for 5 min at 37 °C. Samples were combined by resuspending all beads in 54 µl of LoTE (100 mM NaCl, 0.25% NP-40) plus 6 µl of RNase cocktail (Thermo Scientific, catalog no. AM2286) and incubated at 37 °C for 10 min. Then, 6 µl of 1 M NaOH was added, followed by incubation at 70 °C for 10 min. Supernatant was transferred to a fresh tube and a second elution was performed by resuspending beads in 30 µl of 100 mM NaOH and incubating at 70 °C for 2 min with shaking. The supernatant was combined with the first transfer. Then, 9 µl of 1 M HCl was added to the final sample and DNA clean-up was performed with Zymo DNA concentrator-5 kit (Zymo, catalog no. D4014) following the manufacturer's instructions, eluted in 40 µl of prewarmed water.

PCR amplification. First PCR: 100 µl per sample and split into 2 × 50 µl samples in strip tubes: 40 µl of DNA, 50 µl of 2× Q5 PCR mix (NEB, catalog no. M0492L), 5 µl of each primer at a concentration of 20 µM. PCR program: 98 °C for 30 s, 98 °C for 15 s, 68 °C for 1 min, 72 °C for 1 min, GOTO step 2 nine times, 72 °C for 2 min, HOLD at 4 °C.

PCR primers:. Fwd: CCTACACGACGCTCTTCCGATCTTGTGGAAAGG ACGAAACACCG

Rev: GTTCAGACGTGTGCTCTTCCGATCTCCACTTTTTCAAGTTGATA ACGGACTAGCC

Clean-up was performed with 1.8× AmpureXP beads (Beckman Coulter, catalog no. A63881) according to the manufacturer's instructions, eluted in 40 µl of water for the second PCR input.

Second PCR: 100 µl per sample was split into 2 × 50 µl reactions in strip tubes: 40 µl of DNA elution from the first bead clean-up, 50 µl of 2× Q5 mix, 5 µl each of 20 µM Illumina sequencing primers. PCR program: 98 °C for 30 s, 98 °C for 15 s, 68 °C for 1 min, 72 °C for 1 min, GOTO step 2 six times, 72 °C for 2 min, HOLD at 4 °C. Bead clean-up was performed with 1.4× AmpureXP beads according to the manufacturer's instructions. Elution was performed in 20 µl of water. Library size (~260 bp) and concentration were calculated using a D1000 Tapestation (Agilent, catalog no. 5067-5582) and sequenced to 2 million reads per library on the HiSeq 4000 in single-end 75-bp mode.

siRNA transfections. Well plates were coated with 0.001% w/v PDL and incubated overnight at 37 °C. Immediately before cell plating, the PDL was aspirated and the wells were washed twice with 1× PBS. For imaging in 384-well plates (PerkinElmer, catalog no. 6057300), 4.5×10^3 HEK293T-G3BP1-GFP[32] or HEK293T cells were reverse transfected using 10 nM of siRNA (Dharmacon On-TARGETplus SMARTpool) and Lipofectamine RNAiMax (Invitrogen, catalog no. 13778), according to the manufacturer's protocol, per well. Similarly, 2.25×10^5 HEK293T cells were reverse transfected with siRNAs in 12-well plates for protein lysate collection. After 48 h, stress granules were induced by adding sodium arsenite diluted in DMEM with 10% FBS to a final concentration of 500 µM and incubated

for 1 h at 37 °C. Cells intended for imaging were then fixed by adding 24% PFA to each well to a final concentration of 4% and incubated for 90 min at room temperature. Three washes with 1× PBS were performed to remove PFA. HEK293T cells were immunostained for G3BP1 as described in Cell stress treatment and antibody staining. For UBAP2L co-stainings, primary antibodies 1:1,000 mouse anti-G3BP1 (Millipore, catalog no. 05-1938, RRID:AB_11214423) with 1:500 rabbit anti-UBAP2L (Bethyl, catalog no. A300-533A, RRID:AB_477953) and secondary antibodies 1:1,000 Alexa Fluor 488 goat anti-mouse (Invitrogen, catalog no. A11029, RRID:AB_138404), 1:1,000 Alexa Fluor 555 goat anti-rabbit (Invitrogen, catalog no. A21429, RRID: AB_141761) were used. Nuclei were stained with DAPI (1:5,000 v/v in PBS) for 30 min at room temperature. Cells were washed once with 1× PBS before being preserved in 50% v/v glycerol diluted in 1× PBS.

Imaging of siRNA knockdown in a 384-well plate. Plates were imaged using a Nikon Eclipse Ti2 microscope system operated with NIS Elements High Content software (Nikon). A ×20 (0.75 numerical aperture) objective was used to collect an 8-µm focal range with eight *z* slices for each of the four views acquired per well. The lasers used were 395 nm, 470 nm and 555 nm for DAPI, GFP and RFP, respectively.

Western blot analysis for RBP knockdown. Cells were collected from 12-well plates and pelleted in ice-cold PBS. Pellets were resuspended in 100 µl of RIPA buffer (Sigma, catalog no. R0278) supplemented with Protease Inhibitor (Sigma, catalog no. 539134). Total protein was quantified with the BCA assay (Thermo Scientific, catalog no. 23225) and 20 µg was run on 4%–12% Bis–Tris gel (Thermo Scientific, catalog no. NP0322). Primary antibodies were diluted at 1:1,000 (1:4,000 for GAPDH) in 5% milk–TBST and probed overnight at 4 °C: EIF2AK1 (Bethyl, catalog no. A302-685A, RRID:AB_10754970), PUF60 (Bethyl, catalog no. A302-817A, RRID:AB_10631036), ZCCHC14 (Bethyl, catalog no. A303-096A, RRID:AB_10895018), SNRNP200 (Bethyl, catalog no. A303453A, RRID:AB_10949362), GAPDH (Abcam, catalog no. ab8245, RRID:AB_2107448). Secondary antibodies were diluted at 1:4,000 in 5% milk–TBST and probed for 2 h at room temperature (rabbit secondary (Rockland, catalog no. 18-8816-31, RRID:AB_2610847), mouse secondary (Rockland, catalog no. 18-8817-30, RRID:AB_2610849)). Visualization was performed with ECL and film.

PPI interaction. The human PPI data were retrieved from the BioPlex project (BioPlex v.2.0), Mentha dataset (v.2018-01-08) and proximity-based proteomic studies of stress granule components[35]. The local PPI network of the protein of interest was presented as an undirected and unweighted graph, with each protein as a node and each interaction as an edge. The RBP annotations were collected from several RBP discovery studies[37,55–62] and gene ontology databases, where we retrieved the proteins under the gene ontology term of 'RNA binding' (GO:0003723) and its descendent terms from the AmiGO 2 database (version released in July 2016).

Statistical analysis. Analysis of images from siRNA knockdown (KD) validation experiments was performed from $n = 3$ cell culture well replicates per condition (four images taken per well), with $P < 0.05$ (95% confidence interval) as determined by an unpaired two-tailed *t*-test (d.f. = 4). Data points are presented as mean ±s.d. of each independent experiment.

Reporting Summary. Further information on research design is available in the Nature Research Reporting Summary linked to this article.

Data availability

Sequencing data available under GEO accession GSE139815. RBP CRISPR plasmid library is available on Addgene (141438). Protein–protein interaction data used in this study are curated from Mentha (v.2018-01-08) (https://mentha.uniroma2.it/doDownload.php?file=2018-01-08.zip) and BioPlex v.2.0 (https://bioplex.hms.harvard.edu/data/BioPlex_interactionList_v2.tsv). Any additional data that support the findings of this study are available from the corresponding author upon reasonable request.

Code availability

CRaft-ID software available at https://github.com/YeoLab/CRaftID.

References

50. Tan, F. E. et al. A transcriptome-wide translational program defined by LIN28B expression level. *Mol. Cell* **73**, 304–313.e3 (2019).
51. Sanjana, N. E., Shalem, O. & Zhang, F. Improved vectors and genome-wide libraries for CRISPR screening. *Nat. Methods* **11**, 783–784 (2014).
52. DiSalvo, M. et al. Characterization of tensioned PDMS membranes for imaging cytometry on microraft arrays. *Anal. Chem.* **90**, 4792–4800 (2018).
53. Cao, Q. et al. CRISPR-FOCUS: a web server for designing focused CRISPR screening experiments. *PLoS ONE* **12**, e0184281 (2017).
54. Attayek, P. J. et al. Array-based platform to select, release, and capture Epstein–Barr virus-infected cells based on intercellular adhesion. *Anal. Chem.* **87**, 12281–12289 (2015).
55. Baltz, A. G. et al. The mRNA-bound proteome and its global occupancy profile on protein-coding transcripts. *Mol. Cell* **46**, 674–690 (2012).
56. Castello, A. et al. Insights into RNA biology from an atlas of mammalian mRNA-binding proteins. *Cell* **149**, 1393–1406 (2012).
57. Castello, A. et al. Comprehensive identification of RNA-binding domains in human cells. *Mol. Cell* **63**, 696–710 (2016).
58. Beckmann, B. M. et al. The RNA-binding proteomes from yeast to man harbour conserved enigmRBPs. *Nat. Commun.* **6**, 10127 (2015).
59. Conrad, T. et al. Serial interactome capture of the human cell nucleus. *Nat. Commun.* **7**, 11212 (2016).
60. Sundararaman, B. et al. Resources for the comprehensive discovery of functional RNA elements. *Mol. Cell* **61**, 903–913 (2016).
61. Trendel, J. et al. The human RNA-binding proteome and its dynamics during translational arrest. *Cell* **176**, 391–403.e19 (2019).
62. Queiroz, R. M. L. et al. Comprehensive identification of RNA–protein interactions in any organism using orthogonal organic phase separation (OOPS). *Nat. Biotechnol.* **37**, 169–178 (2019).

Acknowledgements

We thank S. Gebhart and N. Trotta from Cell Microsystems for extensive consultation and troubleshooting support on this project. We thank Yeo laboratory members S. Markmiller for the HEK293T-G3BP1-GFP cell line and F. Tan for the PiggyBAC shuttle vectors. We acknowledge Yeo laboratory members S. Markmiller, M. Perelis, J. Nussbacher, A. Smargon, M. Corley and E. Boyle for critical reading of the manuscript. We thank the members of the Nikon Imaging Center at UC San Diego for help with imaging experiments. E.C.W. and A.Q.V were supported by the National Science Foundation Graduate Research Fellowship. E.C.W. and N.A. were supported in part by a Ruth L. Kirschstein Institutional National Research Award from the National Institute for General Medical Sciences, T32 GM008666. J.M.E. is supported by the Ruth L. Kirschstein F31 National Research Service Award (F31 CA217173) and Cancer Systems Biology Training Program (P50 GM085764 and U54 CA209891). M.D. is supported by the Ruth L. Kirschstein F31 National Research Service Award (F31 CA206233). E.L.V. is supported by the National Human Genome Research Institute (K99HG009530). This work is partially supported by NIH grants HG004659 and NS103172 to G.W.Y and NIH grant EY024556 to N.L.A.

Author contributions

E.C.W., A.Q.V. and G.W.Y conceptualized the project. E.L.V. designed the CRISPR library. J.M.E. cloned the CRISPR library and performed viral infections. A.Q.V. optimized cell plating on microraft arrays. E.C.W. wrote analysis software and performed targeted library preparation. M.D. assisted with confocal imaging and fabricated microraft arrays. A.A.S. and E.L.V. designed the bulk CRISPR library preparation method. N.A. and A.Q.V. implemented neural network analysis. W.J. performed PPI analyses. A.Q.V. and E.C.W. performed validation experiments. E.C.W., A.Q.V. and G.W.Y. wrote the manuscript. N.L.A. and G.W.Y supervised the project.

Competing interests

G.W.Y. is co-founder, member of the Board of Directors, on the SAB, equity holder and paid consultant for Locana and Eclipse BioInnovations. G.W.Y is a visiting professor at the National University of Singapore. E.L.V. is co-founder, member of the Board of Directors, on the SAB, equity holder and paid consultant for Eclipse BioInnovations. The interests of G.W.Y. and E.L.V. have been reviewed and approved by the University of California, San Diego in accordance with its conflict of interest policies. N.L.A. is a co-founder, on the SAB, equity holder and paid consultant for Altis Biosystems and a co-founder and equity holder in Cell Microsystems. The interests of N.L.A. have been reviewed and approved by the University of North Carolina, Chapel Hill through 1 November 2019 and by University of Washington, Seattle as of 1 November 2019 in accordance with their conflict of interest policies. The authors declare no other competing interests.

Additional information

Extended data is available for this paper at https://doi.org/10.1038/s41592-020-0826-8.

Supplementary information is available for this paper at https://doi.org/10.1038/s41592-020-0826-8.

Correspondence and requests for materials should be addressed to G.W.Y.

Peer review information Rita Strack was the primary editor on this article and managed its editorial process and peer review in collaboration with the rest of the editorial team.

Reprints and permissions information is available at www.nature.com/reprints.

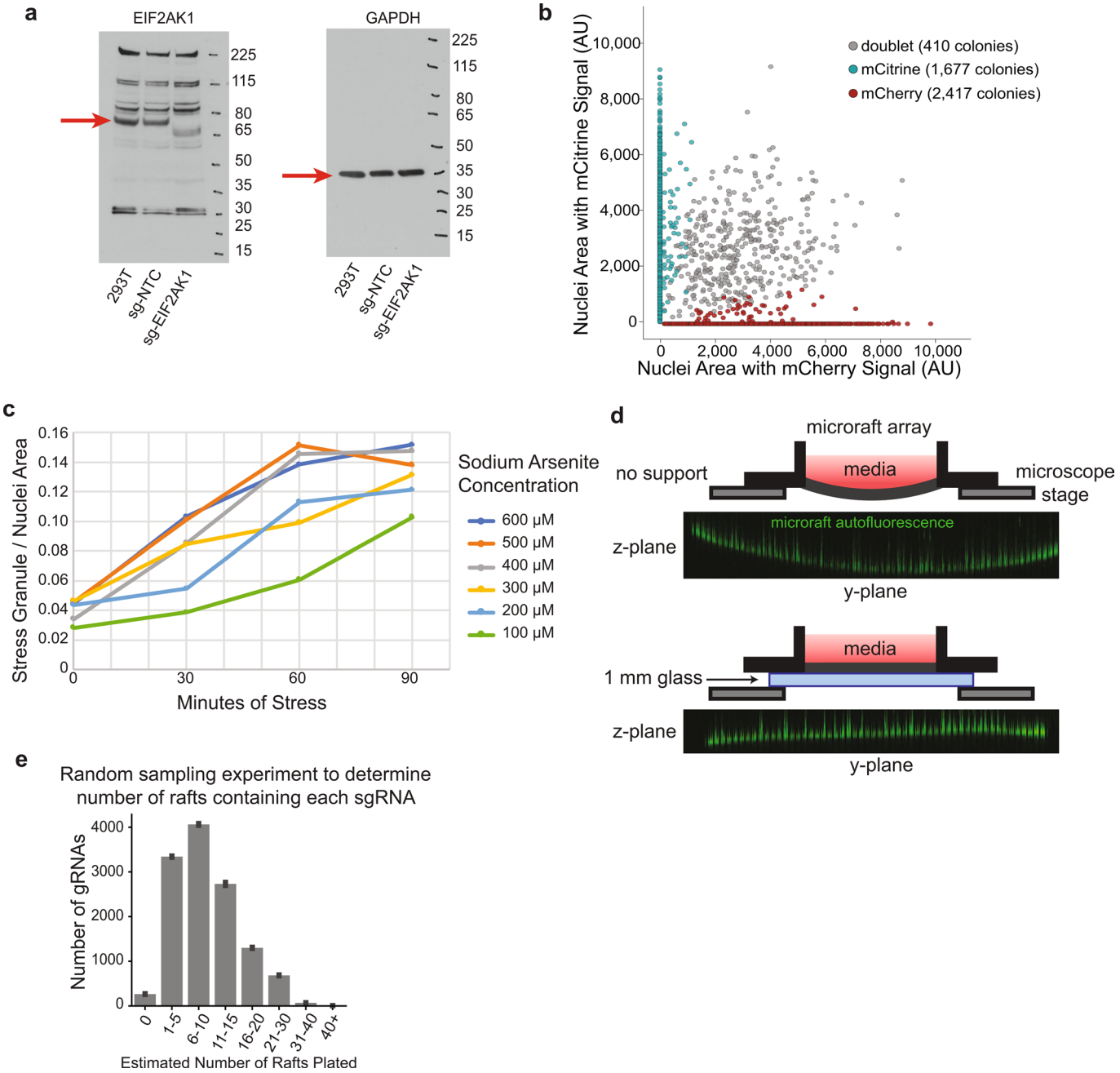

Extended Data Fig. 1 | Optimization of microraft arrays for stress granule quantification. a, Uncropped Western blots measuring EIF2AK1 protein expression in cells infected with sg-NTC (nontargeting control), sg-*EIF2AK1*, or uninfected control cells (293 T). (n = 1) **b**, Scatterplot of mCherry and mCitrine area measured in the nuclei of all colonies detected on a microraft array. Colonies that contain fluorescent signal from both channels in more than 10% of the total nuclei area are determined as doublets (gray). **c**, Time-course analysis of stress granule formation in HEK293T cells under multiple sodium arsenite concentrations measured in 30-minute intervals. Stress granule area is quantified as G3BP1(+) cytoplasmic puncta across n = 1 image. **d**, Top, schematic of microraft array without glass-back support. Orthogonal view of autofluorescence (green) in microrafts across PDMS array after imaging with high laser power. Bottom, diagram of microraft array with 1 mm glass support with orthogonal view of autofluorescent microrafts after imaging with high laser power (green). **e**, Random sampling to estimate plating frequency of sgRNAs on rafts in this screen. Given the relative abundances of sgRNAs on day 7 and the total number of colonies plated (~120,000), random sampling was used to estimate the number of rafts that contain each sgRNA (x-axis), binned in counts of 5. Bars are the average of n = 10 random samplings with error bars displaying standard deviation.

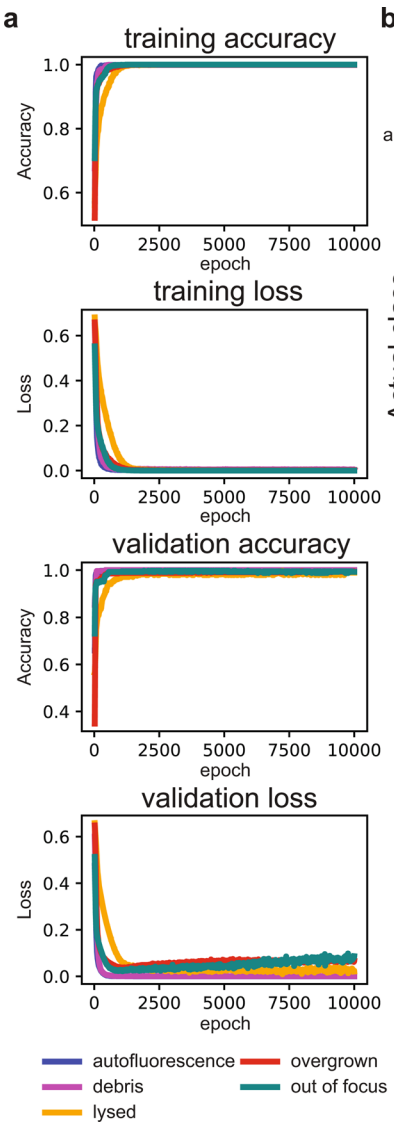

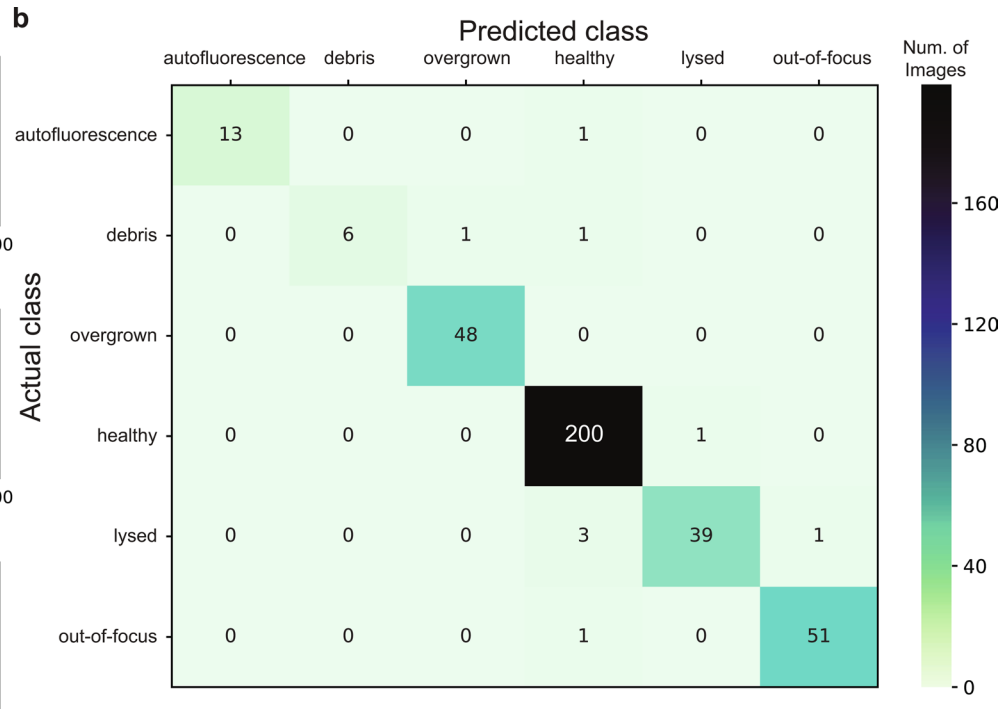

	Class-specific precision	Class-specific recall	F1-score	n
autofluorescence	1.00	0.93	0.96	14
debris	1.00	0.75	0.86	8
overgrown	0.98	1.00	0.99	48
healthy	0.97	0.99	0.98	200
lysed	0.97	0.91	0.94	43
out-of-focus	0.98	0.98	0.98	52
avg / total	0.98	0.98	0.97	365

Extended Data Fig. 2 | Performance of classifiers in image filtering model. a, Learning curves for each binary classifier for 10,000 epochs of training. **b**, Top, confusion matrix for 365 test images comparing the overall model's predicted classifications for each image with its ground-truth. Bottom, average precision rate, recall rate (true positive rate), F1-scores (harmonic mean of precision and recall), and number of images (n) for each binary classifier.

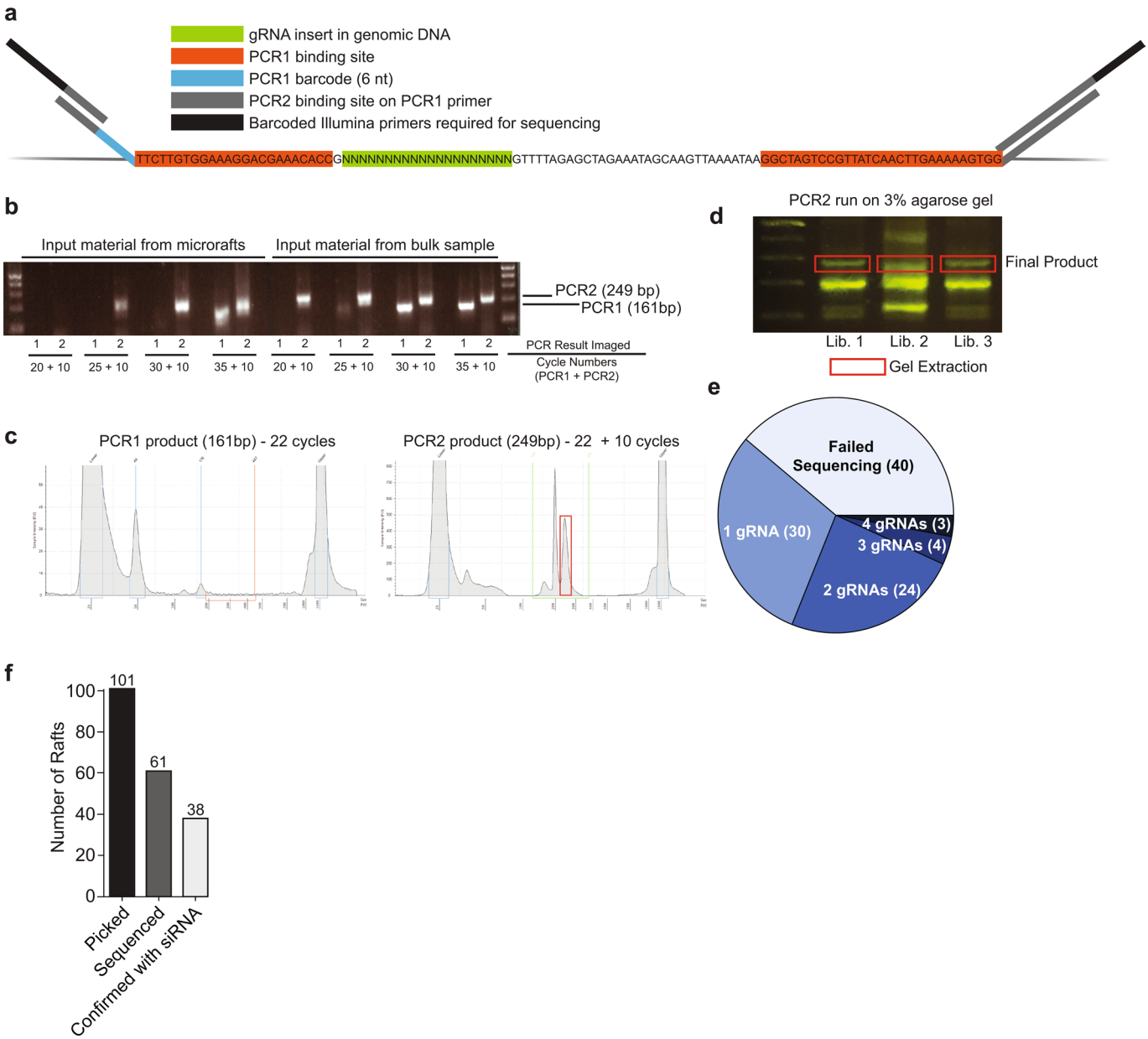

Extended Data Fig. 3 | Library preparation scheme to sequence sgRNA infected in colonies. a, Schematic of PCR barcoding design targeting common regions flanking the sgRNA insert. **b**, Agarose gel of PCR products with increasing cycle numbers to determine the minimum number of PCR cycles required to amplify a product for sequencing. Input material from bulk sample is used as a positive control. All rafts sequenced in this study were amplified with 22 cycles for PCR1 and 10 cycles for PCR2 (n = 213 total, 173 successful). **c**, TapeStation results of PCR products for one representative library containing four pooled microrafts. **d**, Agarose gel of PCR2 product for three representative libraries, each containing four pooled microrafts. Gel extraction was used to isolate the product of interest (red box) from a total of n = 32 libraries. **e**, Summary of the number of sgRNAs identified from each isolated cell colony. **f**, Bar chart of the total number of rafts picked, sequenced, and confirmed by siRNA depletion.

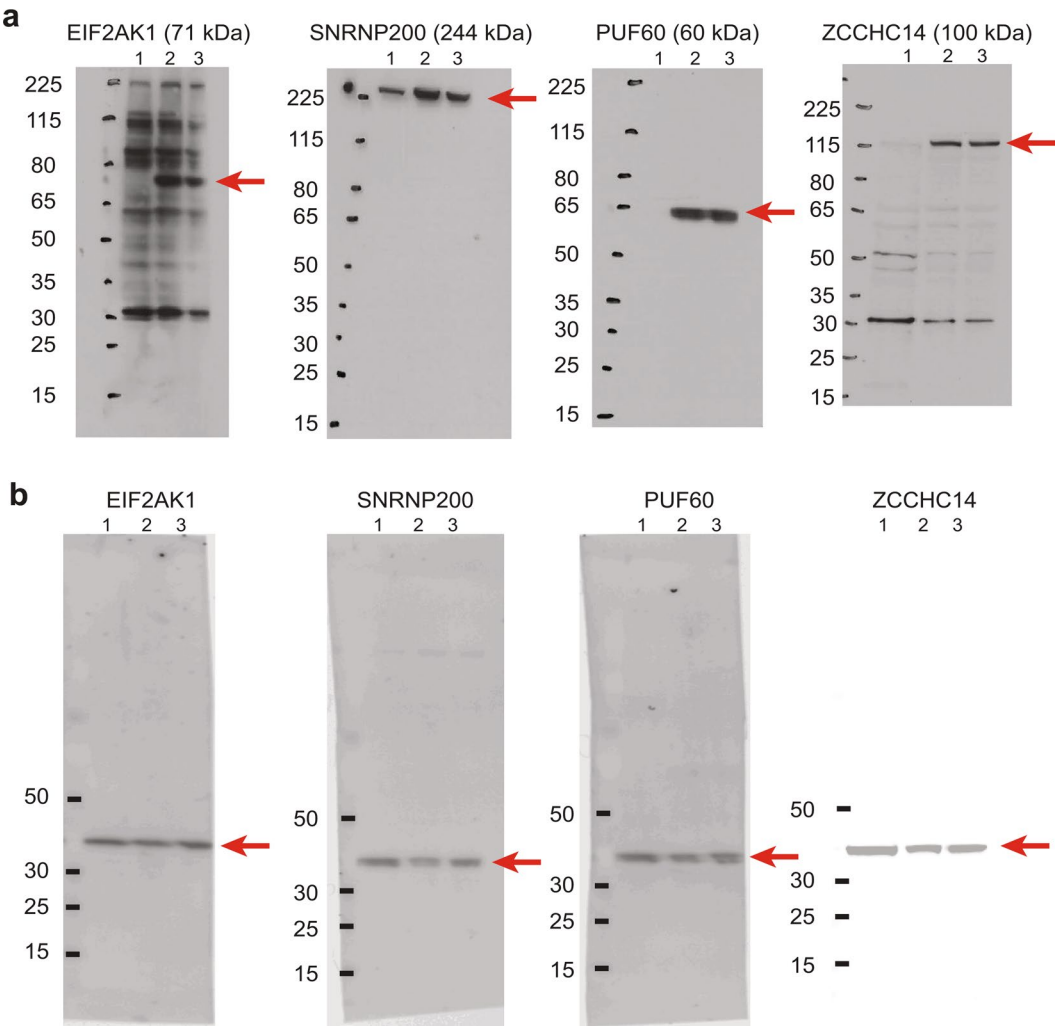

Extended Data Fig. 4 | Uncropped Western blots for siRNA knock-down experiments. a, Samples with knock-down of each protein (labeled above) compared to nontargeting control and untransfected sample. 1 - si-KD targeting, 2 - si-Nontargeting control, 3 - Untransfected HEK293T cells. **b**, GAPDH blots for each respective sample tested in panel a using antibodies of the opposite species on the same membrane.

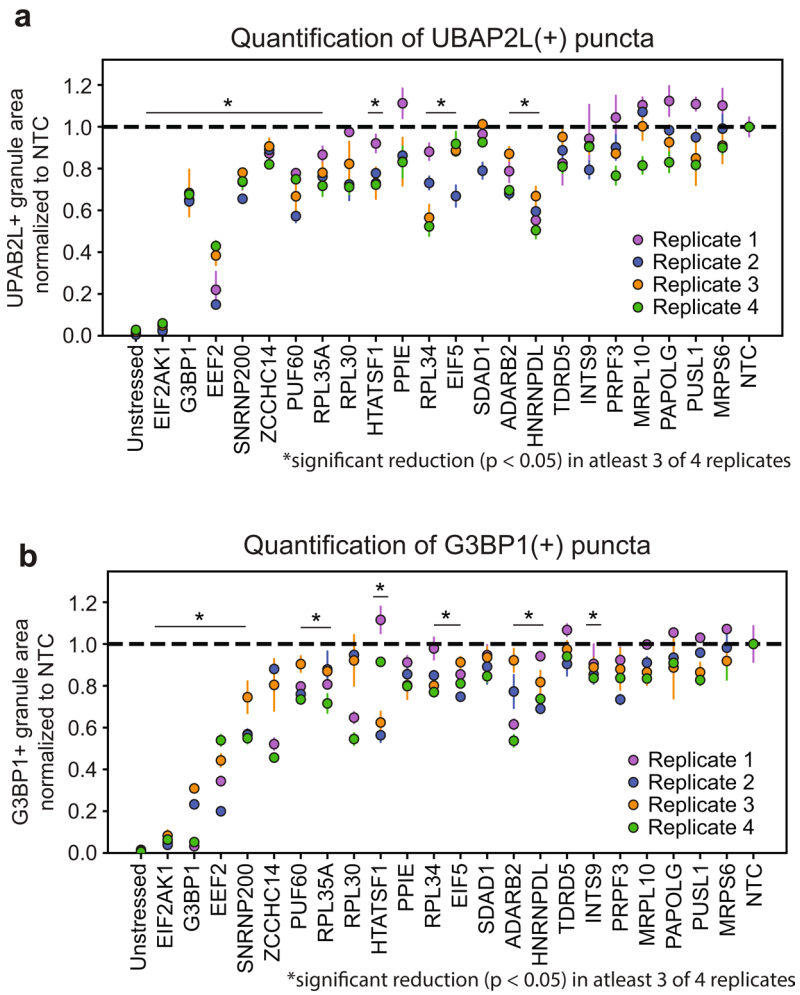

Extended Data Fig. 5 | Depletion of stress-granule regulatory proteins also reduces UBAP2L puncta formation. a, siRNA depletion of target RBPs. UBAP2L(+) granule/nuclei area was normalized to the nontargeting control (NTC) for each experiment. RBPs are ordered in order of appearance in Fig. 3c. *RBPs that had significant reduction ($P < 0.05$, unpaired two-tailed t test, d.f. = 4, 95% confidence interval) of UBAP2L (+) granule area relative to NTC in at least 3 of the 4 biological replicates. Data are mean ± s.d. across n = 3 wells/condition (4 images/well). **b**, G3BP1(+) granule/nuclei area from respective wells measured in panel a. Values are normalized to nontargeting control (NTC) for each experiment. *RBPs that had significant reduction ($P < 0.05$, unpaired two-tailed t test, d.f. = 4, 95% confidence interval) of UBAP2L (+) granule area relative to NTC in at least 3 of the 4 biological replicates. Data are mean ± s.d. across n = 3 wells/condition (4 images/well).

nature research

Corresponding author(s): Gene Yeo

Last updated by author(s): 03/03/2020

Reporting Summary

Nature Research wishes to improve the reproducibility of the work that we publish. This form provides structure for consistency and transparency in reporting. For further information on Nature Research policies, see Authors & Referees and the Editorial Policy Checklist.

Statistics

For all statistical analyses, confirm that the following items are present in the figure legend, table legend, main text, or Methods section.

n/a	Confirmed
☐	☒ The exact sample size (*n*) for each experimental group/condition, given as a discrete number and unit of measurement
☐	☒ A statement on whether measurements were taken from distinct samples or whether the same sample was measured repeatedly
☐	☒ The statistical test(s) used AND whether they are one- or two-sided *Only common tests should be described solely by name; describe more complex techniques in the Methods section.*
☒	☐ A description of all covariates tested
☒	☐ A description of any assumptions or corrections, such as tests of normality and adjustment for multiple comparisons
☐	☒ A full description of the statistical parameters including central tendency (e.g. means) or other basic estimates (e.g. regression coefficient) AND variation (e.g. standard deviation) or associated estimates of uncertainty (e.g. confidence intervals)
☐	☒ For null hypothesis testing, the test statistic (e.g. *F*, *t*, *r*) with confidence intervals, effect sizes, degrees of freedom and *P* value noted *Give P values as exact values whenever suitable.*
☒	☐ For Bayesian analysis, information on the choice of priors and Markov chain Monte Carlo settings
☒	☐ For hierarchical and complex designs, identification of the appropriate level for tests and full reporting of outcomes
☒	☐ Estimates of effect sizes (e.g. Cohen's *d*, Pearson's *r*), indicating how they were calculated

Our web collection on statistics for biologists contains articles on many of the points above.

Software and code

Policy information about availability of computer code

Data collection	Microscopy imaging for positioning the microneedle was performed using previously published and documented MATLAB scripts for microraft array imaging (doi:10.1021/acs.analchem.8b00176). These scripts were executed using MATLAB 2018A (Math Works, Natick, MA) and Micro-Manager Version 1.4.22 (Vale Labs, San Francisco, CA, open-source and available https://micro-manager.org/). The microneedle motor was actuated using the Adafruit Motor Shield V2 library (Adafruit Industries, New York, NY, open-source and available at https://github.com/adafruit/Adafruit_Motor_Shield_V2_Library) and the MATLAB 2018A Support Package for Arduino Hardware. Images acquired on Nikon microscope using NIS Element High Content (HC) analysis package (ver5.20.02) Images captured on Olympus microscope were done using Olympus software FV31S-SW (ver2.1.1.98)
Data analysis	MaGeCk was used to process data for lentiCRISPR bulk samples to quantify sgRNA abundances. Analysis of all other imaging and sequencing data was performed using open-source CRaft-ID software written for this paper (https://github.com/YeoLab/CRaftID). Stress granule and nuclei were segmented and quantified using CellProfiler(v3.0.0)

For manuscripts utilizing custom algorithms or software that are central to the research but not yet described in published literature, software must be made available to editors/reviewers. We strongly encourage code deposition in a community repository (e.g. GitHub). See the Nature Research guidelines for submitting code & software for further information.

Data

Policy information about availability of data

All manuscripts must include a data availability statement. This statement should provide the following information, where applicable:

- Accession codes, unique identifiers, or web links for publicly available datasets
- A list of figures that have associated raw data
- A description of any restrictions on data availability

Sequencing data available under GEO accession #GSE139815. Protein-protein interaction data used in this study are curated from Mentha (version 2018-01-08)

(https://mentha.uniroma2.it/doDownload.php?file=2018-01-08.zip) and BioPlex2.0 (https://bioplex.hms.harvard.edu/data/BioPlex_interactionList_v2.tsv). Any additional data that support the findings of this study are available from the corresponding author upon reasonable request.

Field-specific reporting

Please select the one below that is the best fit for your research. If you are not sure, read the appropriate sections before making your selection.

☒ Life sciences ☐ Behavioural & social sciences ☐ Ecological, evolutionary & environmental sciences

For a reference copy of the document with all sections, see nature.com/documents/nr-reporting-summary-flat.pdf

Life sciences study design

All studies must disclose on these points even when the disclosure is negative.

Sample size	No statistical tests were used to predetermine sample size. All validations by siRNA were performed with multiple replicates (3/experiment) and wells were imaged with four fields of view for a total of 12 images per condition. Sample size numbers are listed in figure legends. Sample sizes for these experiments were chosen based upon field standards and prior knowledge of experimental variation.
Data exclusions	No data exclusions.
Replication	siRNA validation experiments were performed using three (fig 3c) or four (Ext Data 5b) independent experimental replicates (as indicated in the figure legends). Each independent experiment included biological and technical replicates as outlined in legends and methods.
Randomization	Samples were not randomized. Our experimental workflow did not allow/need randomization.
Blinding	No blinding was performed in these experiments. Because many independent investigators were performing experiment independently, blinding was not necessary.

Reporting for specific materials, systems and methods

We require information from authors about some types of materials, experimental systems and methods used in many studies. Here, indicate whether each material, system or method listed is relevant to your study. If you are not sure if a list item applies to your research, read the appropriate section before selecting a response.

Materials & experimental systems

n/a	Involved in the study
☐	☒ Antibodies
☐	☒ Eukaryotic cell lines
☒	☐ Palaeontology
☒	☐ Animals and other organisms
☒	☐ Human research participants
☒	☐ Clinical data

Methods

n/a	Involved in the study
☒	☐ ChIP-seq
☒	☐ Flow cytometry
☒	☐ MRI-based neuroimaging

Antibodies

Antibodies used	Immunofluorescence: G3BP1 (MBL, cat. no. RN048PW, RRID:AB_10794608, lot 004). Used at 1:1000 G3BP1 (Millipore, cat. no. 05-1938, RRID:AB_11214423, clone 14E5-G9, lot 3221518). Used at 1:1000 UBAP2L (Bethyl, cat. no. A300-533A, RRID:AB_477953, lot A300-533A-2). Used at 1:500 AlexaFluor 488 goat anti-mouse (Invitrogen, cat. no. A11029, RRID:AB_138404, lot 1704586). Used at 1:1000 Alexa Fluor 555 goat anti-rabbit (Invitrogen, cat. no. #A21429, RRID:AB_141761, lot 1715464). Used at 1:1000 Alexa Fluor 633 goat anti-rabbit (Invitrogen, cat. no. #A21070, RRID:AB_2535731, lot 1700326). Used at 1:1000 Western Blot: EIF2AK1 (Bethyl, cat. no. A302-685A, RRID:AB_10754970, lot A302-685A-1). Used at 1:1000 PUF60 (Bethyl, cat. no. A302-817A, RRID:AB_10631036, lot A302-817A-1). Used at 1:1000 ZCCHC14 (Bethyl, cat. no. A303-096A, RRID:AB_10895018, lot A303-096A-1). Used at 1:1000 SNRNP200 (Bethyl, cat. no. A303453A, RRID:AB_10949362, lot A303453A-1). Used at 1:1000 GAPDH (Abcam, cat. no. ab8245, RRID:AB_2107448, clone 6C5, lot GR3275542-1). Used at 1:4000 Rabbit IgG HRP Secondary (Rockland, cat. no. 18-8816-31, RRID:AB_2610847, lot 40107). Used at 1:4000 Mouse IgG HRP Secondary (Rockland, cat. no. 18-8817-30, RRID:AB_2610849, lot 38282). Used at 1:4000
Validation	All antibodies used in this study were validated by the vendor and are cited by multiple papers: G3BP1 (MBL) - validated in human cell lines in multiple publications: doi:10.1016/j.cell.2017.12.032, doi:10.1016/

j.neuron.2019.05.048, doi:10.1016/j.celrep.2019.04.015. Also validated in this study where KD of G3BP1 by siRNA reduces IF signal (fig. 3c).
G3BP1 (Millipore) - validated in human cell lines in multiple publications: doi:10.1016/j.cell.2017.12.032 (2018), doi:10.1016/j.celrep.2019.04.015. Also validated in this study where KD of G3BP1 by siRNA reduces IF signal (Ext Data fig. 5b).
UBAP2L (Bethyl) - validated in human cell lines in the publication: doi:10.1016/j.celrep.2019.04.015. Also validated by IP and WB by the ENCODE Project (www.encodeproject.org) in human cell line where cells with targeted protein KD were evaluated against WT control.
AlexaFluor 488 goat anti-mouse, AlexaFluor 555 goat anti-rabbit, AlexaFluor 633 goat anti-rabbit (Invitrogen) - antibodies were validated by the company. Refer to company website for detailed validation analysis
EIF2AK1 (Bethyl) - validated by manufacturer; refer to company website for detailed validation analysis. Also validated in this study where KO of EIF2AK1 by CRISPR results in loss of protein band by WB signal (Ext Data fig. 1a).
PUF60 (Bethyl) - validated on manufacturer's webpage and validated by the ENCODE Project (www.encodeproject.org) in multiple human cell lines where cells with targeted protein KD were evaluated against WT control.
ZCCHC14 (Bethyl) - validated by manufacturer; refer to company website for detailed validation analysis. Also validated in this study where KD of ZCCHC14 by siRNA results in reduced protein signal by WB (fig. 3d)
SNRNP200 (Bethyl) - validated on manufacturer's webpage and validated by the ENCODE Project (www.encodeproject.org) in multiple human cell lines where cells with targeted protein KD were evaluated against WT control.
GAPDH (Abcam) - validated by manufacture and many publications listed on manufacturer's webpage.
Rabbit IgG HRP Secondary (Rockland) - validated by company. "Reactivity is observed against native Rabbit IgG by both Western blot and ELISA." Refer to company website for detailed validation analysis and references.
Mouse IgG HRP Secondary (Rockland) - validated by company. "Reactivity is observed against native Mouse IgG by both Western blot and ELISA." Refer to company website for detailed validation analysis and references.

Eukaryotic cell lines

Policy information about cell lines

Cell line source(s)	Lenti-X HEK293T (HEK293XT) cells (Clonetech, cat. no. 632180); HEK293T (ATCC, cat. no. CRL-3216); HEK293-G3BP1-GFP (gifted from Sebastian Markmiller, doi:10.1016/j.cell.2017.12.032 (2018))
Authentication	All cell lines were commercially supplied and authenticated by their respective suppliers.
Mycoplasma contamination	Cells were tested as negative for mycoplamsa contamination.
Commonly misidentified lines (See ICLAC register)	None were used.